This is the accepted manuscript made available via CHORUS. The article has been published as:

Reach of the high-energy LHC for gluinos and top squarks in SUSY models with light Higgsinos

Howard Baer, Vernon Barger, James S. Gainer, Hasan Serce, and Xerxes Tata

Phys. Rev. D **96**, 115008 — Published 14 December 2017

DOI: 10.1103/PhysRevD.96.115008

UH-511-1281-17

The Reach of the High-Energy LHC for Gluinos and Top Squarks in SUSY Models with Light Higgsinos

Howard Baer[1*], Vernon Barger[2†], James S. Gainer[3‡], Hasan Serce[1§], and Xerxes Tata[3¶]

[1] *Dept. of Physics and Astronomy, University of Oklahoma, Norman, OK 73019, USA*
[2] *Dept. of Physics, University of Wisconsin, Madison, WI 53706, USA*
[3] *Dept. of Physics and Astronomy, University of Hawaii, Honolulu, HI 96822, USA*

Abstract

We examine the top squark (stop) and gluino reach of the proposed 33 TeV energy upgrade of the Large Hadron Collider (LHC33) in the Minimal Supersymmetric Standard Model (MSSM) with light higgsinos and relatively heavy electroweak gauginos. In our analysis, we assume that stops decay to higgsinos via $\tilde{t}_1 \to t\widetilde{Z}_1$, $\tilde{t}_1 \to t\widetilde{Z}_2$ and $\tilde{t}_1 \to b\widetilde{W}_1$ with branching fractions in the ratio 1:1:2 (expected if the decay occurs dominantly via the superpotential Yukawa coupling) while gluinos decay via $\tilde{g} \to t\tilde{t}_1$ or via three-body decays to third generation quarks plus higgsinos. These decay patterns are motivated by models of natural supersymmetry where higgsinos are expected to be close in mass to m_Z, but gluinos may be as heavy as $5-6$ TeV and stops may have masses up to ~ 3 TeV. We devise cuts to optimize the signals from stop and gluino pair production at LHC33. We find that experiments at LHC33 should be able to discover stops with $> 5\sigma$ significance if $m_{\tilde{t}_1} < 2.3$ (2.8) [3.2] TeV for an integrated luminosity of 0.3 (1) [3] ab^{-1}. The corresponding reach for gluinos extends to 5 (5.5) [6] TeV. These results imply that experiments at LHC33 should be able to discover at least one of the stop or gluino pair signals even with an integrated luminosity of 0.3 ab^{-1} for natural SUSY models with no worse than 3% electroweak fine-tuning, and quite likely both gluinos and stops for an integrated luminosity of 3 ab^{-1}.

*Email: baer@ou.edu
†Email: barger@pheno.wisc.edu
‡Email: jgainer@hawaii.edu
§Email: serce@ou.edu
¶Email: tata@phys.hawaii.edu

1 Introduction

In spite of the fact that no direct evidence for superpartners has as yet emerged in Large Hadron Collider (LHC) data, weak scale supersymmetry (SUSY) arguably remains the most promising extension of the Standard Model (SM). The remarkable ultra-violet properties of softly-broken SUSY theories tame the radiative corrections in the Higgs sector and thus provide a resolution [1] of the big hierarchy problem that emerges when the SM is embedded in a Grand Unified Theory (GUT). The MSSM with weak scale superpartners is indirectly supported by several observations: 1) the measured values of gauge couplings, evolved to high scales, appear to unify within the MSSM but not in the SM [2]; 2) the top quark is heavy enough to radiatively drive electroweak symmetry breaking [3]; and 3) the measured Higgs boson mass [4], which could have been as high as several hundred GeV in the SM, lies in the relatively narrow window $m_h \lesssim 135$ GeV (which is support for the MSSM if the MSSM remains valid to $Q \sim M_{\rm GUT}$ [5]).

The search for SUSY has long been one of the important items on the agenda of the ATLAS and CMS experiments at the LHC. The absence of a signal in the data has been interpreted as lower limits on various sparticle masses. The colored superpartners, the squarks and gluinos, are the most stringently constrained, but there are also limits on the masses of electroweakly-produced charginos and neutralinos. For the most part, these limits are obtained in simplified models, usually assuming direct decays to the lightest SUSY particle (LSP) which is taken to be the neutralino. From an analysis of 36 fb^{-1} of data at the (13 TeV) LHC, the ATLAS and CMS collaborations have reported the following 95% CL bounds.

- $m_{\tilde q} \gtrsim 1600$ GeV from a search for squark pair production (assuming 8 degenerate species of light squarks, a massless LSP and decoupled gluinos [6]).
- $m_{\tilde g} \gtrsim 1850 - 2000$ GeV from a search for gluino pair production (assuming $\tilde g \to q\bar q \widetilde Z_1$ with a massless LSP and decoupled squarks [6]).
- $m_{\widetilde W_1} = m_{\widetilde Z_2} \gtrsim 550 - 600$ GeV from a search for wino pair production (assuming $\widetilde W_1 \to \widetilde Z_1 W$ and $\widetilde Z_2 \to \widetilde Z_1 Z$ [7]).

In many models the third generation squarks, especially $\tilde t_1$, are considerably lighter than other squarks. In this case, the gluino would dominantly decay via $\tilde g \to t\bar t \widetilde Z_1$ and perhaps also via $\tilde g \to b\bar b \widetilde Z_1$ or $\tilde g \to tb\widetilde W_1^\pm$. Under this motivation, the LHC collaborations have also searched for signals from stop pair production and also for gluinos dominantly decaying to third generation quarks. Such events would be rich in b-tagged jets. The absence of a signal above backgrounds has led to the following 95% CL bounds (again for nearly massless LSPs).

1. $m_{\tilde t_1} \gtrsim 950 - 1050$ GeV (assuming $\tilde t_1 \to t\widetilde Z_1$ or $Wb\widetilde Z_1$– there is a similar bound on the bottom squark) [8], and
2. $m_{\tilde g} \gtrsim 1960 - 2050$ GeV (assuming $\tilde g \to t\bar t \widetilde Z_1$ [9]).

Considering an LSP with finite mass only mildly degrades these bounds unless the LSP is relatively close in mass to the parent sparticle.

As the LHC continues to accumulate more data, the ATLAS and CMS experiments will probe even larger superpartner masses. With an integrated luminosity of 300 fb^{-1} – expected to be accumulated at $\sqrt{s} = 14$ TeV by the end of LHC Run 3 – experiments should be able to probe gluinos with a 5σ significance out to ~ 1.9 TeV ($\tilde{g} \to q\bar{q}\widetilde{Z}_1$) and stops to about 950 GeV [10, 11]. The 95% CL reach is typically 300-400 GeV higher. At the "High Luminosity LHC" (HL-LHC) where an integrated luminosity of 3000 fb^{-1} is anticipated, these reaches extend to about 2300 GeV (gluino) and 1200 GeV (stop) [10, 11, 12]. In a recent study, we have shown that with stringent selection cuts, the 5σ gluino discovery potential of (the 14 TeV) LHC extends to 2.4 (2.8) TeV, for an integrated luminosity of 300 (3000) fb^{-1} if the gluino decays via $\tilde{g} \to t\tilde{t}_1 \to t\bar{t}\widetilde{Z}_1$ [13].

While colored sparticle searches are usually expected to probe most deeply into SUSY parameter space at hadron colliders, for integrated luminosities larger than 300 fb^{-1} electroweak-ino pair production becomes competitive, or even dominant for the case that the gluino decays democratically into all generations. For instance, wino pair production via $pp \to \widetilde{W}_2(\to W^\pm\widetilde{Z}_{1,2})\widetilde{Z}_4(\to W^\pm\widetilde{W}_1^\mp)X)$ followed by decay to same-sign dibosons ($W^\pm W^\pm$) may probe more deeply into parameter space than gluino production in the well-motivated class of *natural SUSY* models with light higgsinos and gaugino mass unification [14, 15].

If SUSY is not discovered at the HL-LHC, then the search for SUSY may require new facilities. An electron-positron linear collider with $\sqrt{s} > 2\,m_{\rm higgsino}$ is particularly well suited [16] for SUSY discovery since the requirement of light higgsinos has been argued to be a very robust feature of natural SUSY models [17, 18, 19]. In this paper, however, we examine the SUSY reach of the proposed *energy upgrade* of the LHC: a pp collider operating at $\sqrt{s} = 33$ TeV with an anticipated integrated luminosity of ~ 1 ab^{-1}, referred to hereafter as LHC33 [20].[1] We examine in detail the LHC33 discovery reach for gluinos and stop pair production, focussing on the case where $\tilde{g} \to t\tilde{t}_1$ and $\tilde{t}_1 \to t + X$ or $\tilde{t}_1 \to bX$ each with a branching fraction of 50% and where the decay products of X are essentially invisible.[2]

We will defer a detailed discussion of our motivation for focussing on gluino and stop searches (with the assumed decay patterns) until Sec. 5. Briefly, we will see that in a wide variety of natural SUSY models, the gluino and stop masses are *bounded from above* by naturalness conditions and that these superpartners decay as we have assumed. These upper bounds – that $m_{\tilde{g}} \lesssim 5-6$ TeV and $m_{\tilde{t}_1} \lesssim 3$ TeV – imply that these sparticles may well lie beyond the reach of HL-LHC. Moreover, in well-motivated SUSY models such as mirage-mediation with a compressed spectrum of gauginos, electroweak-ino signals may also be beyond the reach of HL-LHC. For a definitive test of natural SUSY at a hadron collider, an energy upgrade to the vicinity of $\sqrt{s} \sim 30$ TeV seems necessary to probe the natural parameter space. We find that experiments at LHC33 will definitively be able to discover at least one of these superpartners over the entire parameter space of natural SUSY models, and both over much of the allowed parameter space. While we find these conclusions highly compelling, the reader who does not subscribe to our naturalness criteria should view this paper instead simply as an analysis of the LHC33 reach for gluino and stop pair production in models with decays to light higgsinos.

[1] We will also consider the scenario where LHC33 obtains 3 ab^{-1} of integrated luminosity.

[2] In a previous study [21] we had shown that the gluino reach of LHC33 extended beyond 5 TeV, the exact value depending on the stop mass. In this paper we re-evaluate the reach while improving our cuts for gluino pair events. Our evaluation of the stop reach is new.

Before proceeding further we should mention how our analysis differs from the one existing study [22] of the reach for gluinos at LHC33 that we are aware of. To our knowledge there is no detailed corresponding study for stops.[3] In Ref. [22] the authors examine the discovery reach of gluinos for various scenarios including $\tilde{g} \to t\tilde{t}_1$ of interest to us. They focus, however, on the same-sign dilepton event channel that is possible if the two (of four) leptonically decaying tops have the same sign of electric charge. The rate for the signal is then suppressed by the square of the leptonic branching fraction for top quark decays, and also by the fact that such events are not possible if $\tilde{t}_1 \to b\widetilde{W}_1$, and the daughters of the chargino are too soft to be efficiently detectable. Our strategy is, instead, to allow the fully inclusive sample of gluino events requiring just hard tagged b-jets and large $E_T^{\rm miss}$ in the events as we did in an earlier analysis for the HL-LHC. We will see that this leads to a significantly larger reach than in Ref. [22].

The remainder of this paper is organized as follows. Sec. 2 explains the procedures used to simulate the relevant signal and background processes and also lists the reactions that we have simulated. Sec. 3 describes the analyses used, in particular explaining how we arrive at our choice of cuts for both the stop and the gluino signal. In Sec. 4, we use these analyses to make projections for the discovery and exclusion reach, in terms of the stop and gluino masses, at LHC33. The implications of these projected discovery and exclusion reaches for natural SUSY models are discussed in Sec. 5. Finally, we summarize our main results and present our conclusions in Sec. 6.

2 Event Simulation

We begin by describing how we simulate gluino and stop signal events at LHC33 as well as the various SM backgrounds listed in Sec. 2.2.

2.1 Event Generation

LHC33 events were generated using MadGraph 2.3.3 [23] interfaced to PYTHIA 6.4.14 [24] via the default MadGraph/PYTHIA interface with default parameters for showering and hadronization. Detector simulation is performed by Delphes using the default Delphes 3.3.0 [25] "CMS" parameter card with the modifications listed below.

1. We set the electromagnetic calorimeter (ECAL) energy resolution to $3\%/\sqrt{E} \oplus 0.5\%$ and the hadronic calorimeter (HCAL) energy resolution to be $80\%/\sqrt{E} \oplus 3\%$ for $|\eta| < 2.6$ and $100\%/\sqrt{E} \oplus 5\%$ for $|\eta| > 2.6$, where "$\oplus$" denotes combination in quadrature. These are typical of the values used for LHC calorimeters and do not assume any significant improvement at LHC33.

2. We turn off the jet energy scale correction.

[3] In Ref. [11] Fig. 1-24 shows that LHC33 should be able to probe stops via the single lepton channel, assuming $\tilde{t} \to t\widetilde{Z}_1$. Unfortunately, no details are given.

3. We utilize the anti-k_T jet algorithm [26] with $R = 0.4$ rather than the default $R = 0.5$. (Jet finding in Delphes is implemented via FastJet [27].) We consider only jets with transverse energy satisfying $E_T(jet) > 50$ GeV and pseudorapidity satisfying $|\eta(jet)| < 3.0$ in our analysis. The choice of $R = 0.4$ in the jet algorithm is made, in part, to facilitate comparison with CMS b-tagging efficiencies [28] described below.

4. We have developed our own module for jet flavor association to implement the "ghost hadron" procedure [29] that allows decayed hadrons to be assigned to jets in an unambiguous manner; we use this module to determine whether jets contain B hadrons. If a jet contains a B hadron (in which the b quark decays at the next step of the decay) with $|\eta| < 3.0$ and $E_T > 15$ GeV, then we identify this b-jet as a "truth b-jet". We tag b-jets with $|\eta| < 1.5$ with an efficiency of 60% and assume that light quark and gluon jets with $|\eta| < 1.5$ can be mistagged as b-jets with a probability of 1/150 for $E_T < 100$ GeV, 1/50 for $E_T > 250$ GeV and a linear interpolation for 100 GeV $< E_T <$ 250 GeV.[4] We have checked [13] that our b-jet tagging algorithm yields good agreement with the b-tagging efficiencies and mistag rates in Ref. [28]. While these b-tagging parameterizations were developed for the (14 TeV) LHC, we expect that they represent reasonable starting points for LHC33 phenomenology. More detailed studies, beyond the scope of this paper, will ultimately be needed to understand b-tagging at LHC33.

5. We do not perform "tau tagging", *i.e.*, identifying objects as taus, as our analyses does not involve the tagging of hadronic taus and we do not want to "lose" b-jets where the B hadron in the jet decays to a tau lepton.

The lepton identification criteria that we adopt are the default for this version of Delphes, namely leptons with $E_T > 10$ GeV and within $|\eta_\ell| < 2.5$ are considered isolated if the sum of the transverse energy of all other objects (tracks, calorimeter towers, etc.) within $\Delta R = 0.5$ of the lepton candidate is less than 10% of the lepton E_T.

2.2 Processes Simulated

As mentioned in Sec. 1, our goal is to map out the LHC33 reach for gluinos and stops, assuming that these are the only colored superpartners that are kinematically accessible. For definiteness, we assume that gluinos decay via $\tilde{g} \to t\tilde{t}_1$, and that the stop decays via $\tilde{t}_1 \to t\widetilde{Z}_{1,2}$ or $\tilde{t}_1 \to b\widetilde{W}_1$ with branching ratios of 0.25, 0.25 and 0.50, respectively. These branching ratios are typical for models with light higgsinos and relatively heavy gauginos, where the decay dominantly occurs via the top quark Yukawa coupling [15]. Unless the bino and wino are fortuitously also rather light, the visible decay products of the daughter $\widetilde{Z}_2$ and $\widetilde{W}_1$ are generally very soft because the higgsino mass gap is typically 5-20 GeV. In our analysis of the LHC33 reach, we will assume that the higgsinos are not detectable in the experimental apparatus. We should thus regard our results as conservative since the additional (especially leptonic) debris from the neutralino and chargino decays could be potentially used to further "beat down" SM backgrounds. The

[4] These values are based on ATLAS studies of b-tagging efficiencies and rejection factors in $t\bar{t}H$ and WH production processes [30].

associated gluino top-squark production cross section is negligible, essentially because the top quark density in the proton is very small.

Gluino pair production at LHC33 thus leads to $tttt + E_T^{\rm miss}$, $tttb + E_T^{\rm miss}$, $ttbb + E_T^{\rm miss}$ and $bbbb + E_T^{\rm miss}$ events, where the $E_T^{\rm miss}$ arises the fact that the daughter higgsinos are essentially invisible. Likewise, stop pair production leads to $tt + E_T^{\rm miss}$, $tb + E_T^{\rm miss}$ and $bb + E_T^{\rm miss}$ events. SUSY events are thus signalled by the production of 2-4 very hard b-jets (not all of which would be tagged as b-jets) and very large $E_T^{\rm miss}$.

The dominant SM backgrounds come from SM processes with top and bottom quarks in the final state, with the physics $E_T^{\rm miss}$ arising primarily from neutrinos from the decays of top quarks and Z bosons. With this in mind, we simulated backgrounds from $t\bar{t}$, $t\bar{t}b\bar{b}$, $t\bar{t}h(\to b\bar{b})$, $b\bar{b}Z$, and $t\bar{t}t\bar{t}$ production and from single top production.[5] In our evaluation of the background from top pair production, we veto $t\bar{t}$ events with more than two truth b-jets, to avoid double counting (as we also explicitly simulate $t\bar{t}b\bar{b}$). When simulating our $t\bar{t}$, $t\bar{t}b\bar{b}$, single top, and $b\bar{b}Z$ backgrounds, we generate events in bins of generator-level missing transverse energy, $E_T^{\rm miss}$. Using weighted events from this procedure yields a more accurate simulation of the high tail of the $E_T^{\rm miss}$ distribution for these background processes, which is essential for determining the rates from background processes after the very hard $E_T^{\rm miss}$ cuts that we use for the extraction of the signal: see Sec. 3.

In our MadGraph simulation, we normalize the $2 \to 2$ pair production cross section for our gluino pair production signals and our stop pair production signals, for various stop and gluino masses, to the NLO + NLL (next-to leading logarithm) values from the LHC SUSY cross section working group [31]. We display these total cross sections, as well as the corresponding cross sections at the (14 TeV) LHC in Fig. 1. We see that $\gtrsim 100$ gluino (stop) pair events should be produced at LHC33 if $m_{\tilde{g}}$ ($m_{\tilde{t}_1}$) < 5 (3) TeV, assuming an integrated luminosity of 1 ab^{-1}. The cross section for our top pair production background was normalized to 5449.6 pb, following ATLAS-CMS recommended predictions[6] [32] for the LHC33, which are ultimately based on Hathor v2.1 [33]. As we were unable to find NLO K-factors for the other background processes, we have used the same K-factor values that we used for the 14 TeV analysis in Ref. [13]. These are 1.3 for $t\bar{t}b\bar{b}$, following Ref. [34][7]; 1.5 for $b\bar{b}Z$ production, following Ref. [36]; 1.27 for the $t\bar{t}t\bar{t}$ backgrounds, following Ref. [37], and 1.11 for single-top cross sections, following the (14 TeV) ATLAS-CMS recommended predictions [38] which are ultimately based on the Hathor v2.1 program [33].

3 Event Selection

In this section, we develop sets of cuts to separate gluino pair and top-squark pair production events from SM backgrounds with the goal of optimizing the reach of LHC33. We first discuss the stop pair signal in Sec. 3.1 and then turn to the gluino pair production signal in Sec. 3.2.

[5] In a previous study at the 14 TeV LHC [13], we had shown that backgrounds from vector boson production ($V+$ jet production and VV+jet production) were very efficiently removed after requiring two hard b-jets and large $E_T^{\rm miss}$.

[6] This is the cross section for a top mass of 173.2 GeV, which we find by interpolation from the provided cross sections.

[7] Larger K-factors for this process are obtained when a dynamic scale choice is not employed [35].

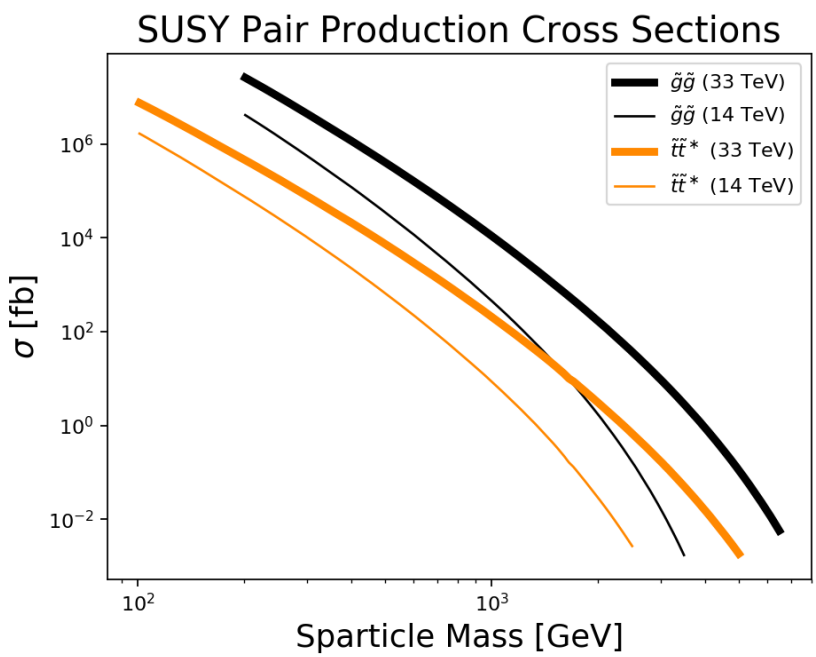

Figure 1: Total NLO+NLL cross sections for gluino (black) and stop (lighter/ orange) production at LHC33 (thick curves) and, for comparison, at the 14 TeV LHC (thin curves).

3.1 Stop Analysis

In order to determine the discovery reach for stops at LHC33, we must first develop a set of cuts to separate the stop pair production signal events from various SM backgrounds. The reach will be approximately optimized by tuning the cuts for the extraction of a signal from a heavy stop. With this in mind and given the stop pair production rate in Fig. 1, we adopt a simplified model benchmark point with $m_{\tilde{t}_1} = 2.75$ TeV, for which $\sigma_{\tilde{t}_1\tilde{t}_1} \sim 300$ ab (corresponding to 100-300 events before analysis cuts depending on the integrated luminosity) to enhance the stop signal over the background. For definiteness, we adopt a higgsino mass parameter $\mu = 150$ GeV, though we expect the results to be only weakly sensitive to this value (as long as $|\mu| \ll m_{\tilde{t}_1}$). The masses of relevant particles are given in Table 1. In the context of this simplified model, we consider only pair production of the (lightest) stop, $pp \to \tilde{t}_1\tilde{t}_1^*$, and we assume that the decays $\tilde{t}_1 \to t\widetilde{Z}_1$, $\tilde{t}_1 \to t\widetilde{Z}_2$, and $\tilde{t}_1 \to b\widetilde{W}_1$ occur in the ratio $1:1:2$.

We use the stop benchmark point that we have adopted to design cuts to separate the SUSY signal from SM backgrounds, showing the relevant distributions at each step. We begin with the following relatively basic cuts:

$$\begin{aligned} n_b &\geq 2, \\ n_\ell &= 0, \\ E_T^{\rm miss} &> \max(750\ {\rm GeV}, 0.2 M_{\rm eff}), \\ E_T(j_1) &> 500\ {\rm GeV}, \end{aligned} \tag{1}$$

parameter	value
$m_{\tilde{t}_1}$	2750.0
$m_{\widetilde{W}_1}$	150.0
$m_{\widetilde{Z}_2}$	150.0
$m_{\widetilde{Z}_1}$	149.0
m_t	173.2

Table 1: Particle masses in GeV units in a natural SUSY [19] simplified model used to obtain the optimized cuts (6) described in the text.

$$\begin{aligned} E_T(j_2) &> 300 \text{ GeV}, \\ S_T &> 0.1, \end{aligned}$$

where n_b is the number of b-tagged jets, n_ℓ is the number of isolated leptons[8] (e or μ), $M_{\rm eff}$ is the scalar sum of the E_T of the (up to) four leading jets and $E_T^{\rm miss}$, and S_T is the transverse sphericity, which is sphericity[9] defined using only transverse quantities. We display the $E_T^{\rm miss}$ distribution after the cuts (1) in Fig. 2 for the signal benchmark point and for the backgrounds considered. For clarity, here and in subsequent figures we do not separately show the background contribution from $t\bar{t}h(\to b\bar{b})$ production. After the final selection cuts detailed below, this contribution is an order of magnitude smaller than that from QCD $t\bar{t}b\bar{b}$ production shown in the figure, and constitutes $\lesssim 1\%$ of the total background to both the stop as well as the gluino signal. As expected, we see that the signal to background ratio (S/B) becomes larger with increasing $E_T^{\rm miss}$. Nonetheless, to maximize the reach we choose cuts to preserve as much signal as possible. Since the signal $E_T^{\rm miss}$ distribution for our benchmark point, with its relatively heavy stop, attains a broad peak at $E_T^{\rm miss} \sim 1500$ GeV, we require

$$E_T^{\rm miss} > 1500 \text{ GeV}. \tag{2}$$

At this stage, $t\bar{t}$ remains the largest contributor to the background.

With the more stringent $E_T^{\rm miss}$ cut (2) we turn our attention to other observables, first focusing on cuts to suppress the dominant $t\bar{t}$ background. Toward this end, we recognize that $t\bar{t}$ production is most likely to yield events with $E_T^{\rm miss} \gg m_t$ if the tops are produced with large transverse momentum, with one top decaying semi-leptonically and the other hadronically. In this case, because the top decay products are strongly boosted, the neutrino from the semi-leptonically decaying top (which gives the bulk of the $E_T^{\rm miss}$) is likely to be aligned with the b-parton jet from the same top, regardless of whether or not it is tagged as a b-jet. This suggests that we examine the distribution of of $\Delta\phi(E_T^{\rm miss},$ nearest jet), the minimum angle

[8]Our isolation criteria (c.f. Sec. 2.1) are rather stringent, so demanding $n_\ell = 0$ removes fewer signal and background events than one naively might expect. However, the main point of this lepton veto is to reduce $t\bar{t}$ backgrounds, which will ultimately be reduced to $\lesssim 0.1$ ab in both our stop and gluino analyses anyway, so making a more stringent lepton veto by loosening the isolation criteria is unlikely to have a greater effect in reducing backgrounds than in reducing signals.

[9]See, *e.g.*, *Collider Physics*, V. Barger and R. J. N. Phillips (Addison Wesley, 1987) for the definition of sphericity.

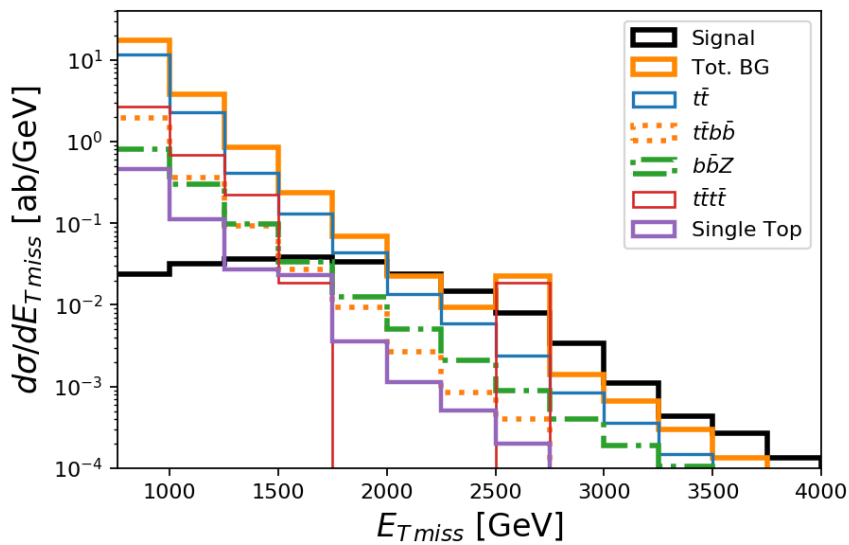

Figure 2: Distribution of $E_T^{\rm miss}$ after initial cuts (1) for a 2.75 TeV stop, as well as for the most relevant backgrounds, namely $t\bar{t}$, $t\bar{t}b\bar{b}$, $b\bar{b}Z$, $t\bar{t}t\bar{t}$ and single top.

between the transverse momenta of any jet and the $E_T^{\rm miss}$ vector in the transverse plane, which we shall henceforth term $\Delta\phi$. While we expect the $t\bar{t}$ background (and to a large extent also $t\bar{t}b\bar{b}$ background) to peak at small $\Delta\phi$, we do not expect this to be the case for the signal since the higgsino directions are not particularly correlated with those of the other daughters of the stop. This distribution is shown in Fig. 3.

We indeed see that removing events with small $\Delta\phi$ values [13, 39] will significantly reduce the background with little effect on the signal. We therefore require an additional analysis cut,

$$\Delta\phi > 30 \text{ degrees}. \tag{3}$$

We see that this cut reduces the background to be smaller than the signal for the benchmark point and that after this cut 95% of the SM background is due to $b\bar{b}Z$ production. To further optimize the signal, we investigate the distribution of the E_T of the leading jet for signal and background in Fig. 4. We show only the total backgound in this and in the following figures. We observe that the background distribution is peaked at somewhat lower values than the signal distribution, suggesting that the additional cut,

$$E_T(j_1) > 1000 \text{ GeV}, \tag{4}$$

will be useful. Finally, after imposing cut (4), we see – from the E_T distribution of the second leading jet for signal and background shown in Fig. 5 – that requiring

$$E_T(j_2) > 600 \text{ GeV}, \tag{5}$$

will further enhance the signal relative to the background. Cuts (1 - 5) together constitute our

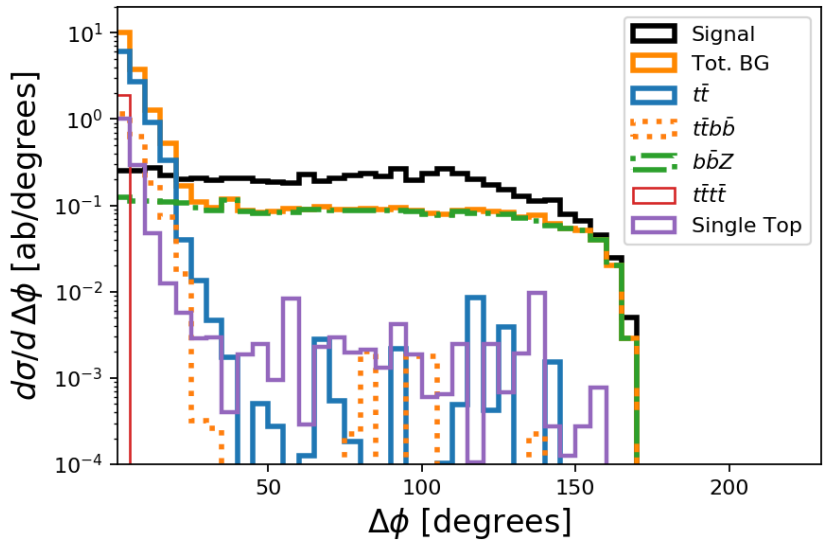

Figure 3: Distribution of $\Delta\phi$ after initial cuts (1) and the subsequent harder $E_T^{\rm miss}$ cut (2) for a 2.75 TeV stop, as well as for the most relevant backgrounds.

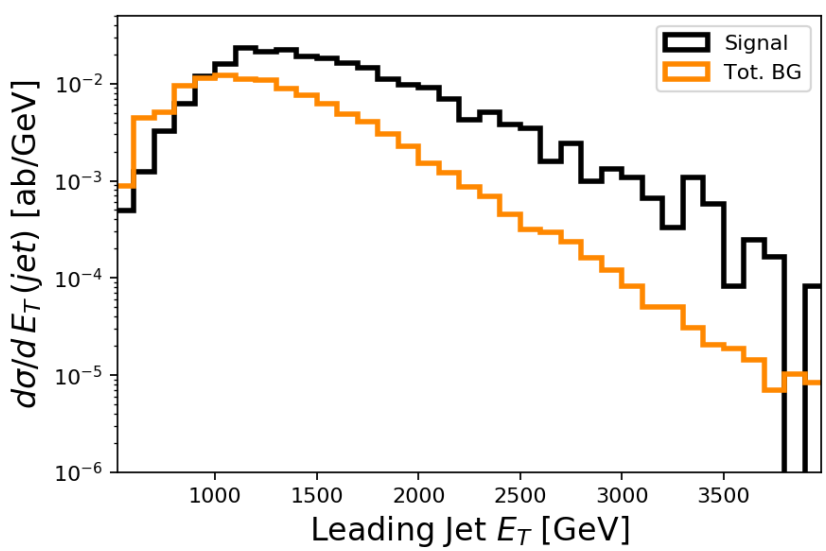

Figure 4: Distribution of leading jet E_T for the signal and for the sum of the backgrounds after initial cuts (1), the subsequent harder $E_T^{\rm miss}$ cut (2), and the $\Delta\phi$ cut (3).

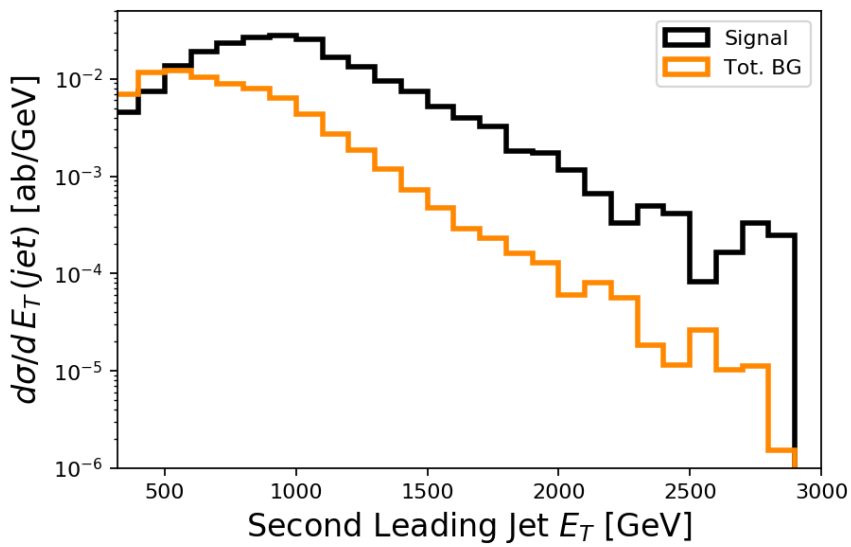

Figure 5: Distribution of second leading jet E_T after initial cuts (1) and the subsequent harder $E_T^{\rm miss}$ cut (2), $\Delta\phi$ cut (3), and leading jet E_T cut (4).

analysis cuts for the stop signal at LHC33. Combining these cuts, we obtain

$$\begin{aligned} n_b &\geq 2, \\ n_\ell &= 0, \\ E_T^{\rm miss} &> \max(1500\ {\rm GeV}, 0.2 M_{\rm eff}), \\ E_T(j_1) &> 1000\ {\rm GeV}, \\ E_T(j_2) &> 600\ {\rm GeV}, \\ S_T &> 0.1, \\ \Delta\phi &> 30\ {\rm degrees}. \end{aligned} \tag{6}$$

After these cuts, the total background cross section is 4.6 ab, as compared to a signal cross section of 18.9 ab for the (2.75 TeV stop) benchmark model. Over 95% of this background is from $b\bar{b}Z$; the cuts have effectively rejected the other backgrounds, in particular $t\bar{t}$. While we will not attempt to optimize our cuts further, as we wish our results to be robust with respect to the details of our simulation, this does suggest that a more aggressive analysis to separate the $b\bar{b}Z$ background from the stop production signal may be possible.

3.2 Gluino Analysis

Next, we turn to the determination of the optimal cuts for gluino discovery. We had seen in a previous study [21] that the LHC33 reach for gluinos extends beyond $\sim$ 5 TeV. Here, we

parameter	value
m_0	11750
$m_{1/2}$	2350
A_0	-18800
$\tan\beta$	10
μ	150
m_A	2350
$m_{\tilde{g}}$	5379.0
$m_{\tilde{t}_1}$	4257.8
$m_{\tilde{t}_2}$	8947.3
$m_{\tilde{b}_1}$	9010.8
$m_{\widetilde{W}_2}$	2020.4
$m_{\widetilde{W}_1}$	161.6
$m_{\widetilde{Z}_4}$	2052.0
$m_{\widetilde{Z}_3}$	1085.6
$m_{\widetilde{Z}_2}$	157.1
$m_{\widetilde{Z}_1}$	152.5
m_h	126.7

Table 2: NUHM2 input parameters and some superpartner masses in GeV units for the *radiatively-driven natural SUSY* [19] benchmark point used to develop the cuts (11) used in our gluino discovery analysis. We take $m_t = 173.2$ GeV.

attempt to choose the gluino analysis cuts to better optimize the reach. Toward this end, we adopt a SUSY benchmark point in the natural NUHM2 model [19] again with $\mu = 150$ GeV, but $m_{\tilde{g}} \sim 5.4$ TeV, so the wino mass is 2 TeV, and the bino mass ~ 1.1 TeV. Other squarks and sleptons are essentially decoupled. Although from Fig. 1 we expect only 30-40 gluino pair events per 1 ab^{-1} at LHC33, we expect that these events will efficiently pass stringent selection cuts to separate them from SM backgrounds with higher efficiency than stop events. This is partly because gluino events are harder, and partly because gluino pair events contain four (rather than two) hard b-parton jets that we can use to reduce the SM background. We will focus our attention on the case where the gluino decays exclusively via $\tilde{g} \to \tilde{t}_1\bar{t}, \tilde{t}_1^* t$. The backgrounds considered are the same as those examined in our stop discovery analyses (Sec. 3.1).

The parameters and relevant mass spectrum for the SUSY benchmark point that we use to develop our cuts for a gluino search at LHC33 are shown in Table 2. We now develop our cuts for gluino discovery, again showing the relevant distributions at each step. We begin with the following relatively basic cuts:

$$\begin{aligned} n_b &\geq 2, \\ n_\ell &= 0, \\ E_T^{\rm miss} &> \max(750\ {\rm GeV}, 0.2 M_{\rm eff}), \\ n_j &\geq 4 \\ E_T(j_i) &> 200\ {\rm GeV},\ (i = 1-4) \end{aligned} \tag{7}$$

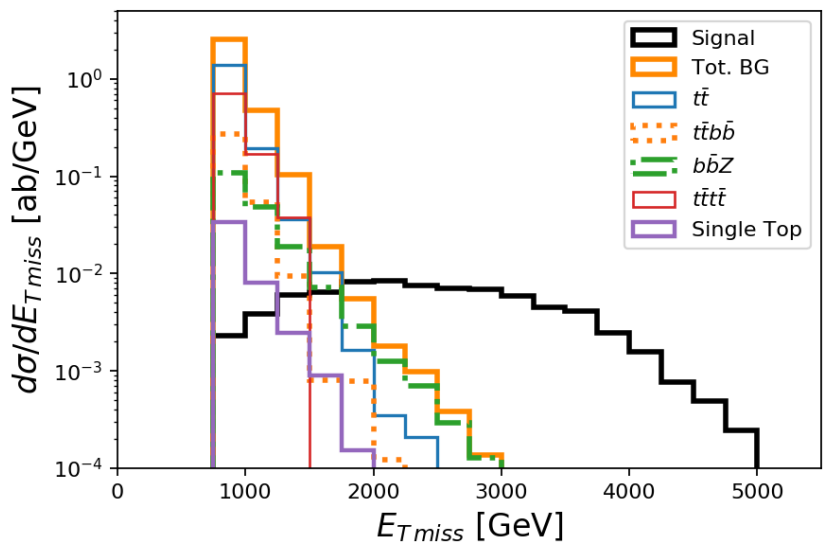

Figure 6: Distribution of $E_T^{\rm miss}$ after initial cuts (7) for the gluino benchmark point in Tab. 2, as well as for the most relevant backgrounds, namely $t\bar{t}$, $t\bar{t}b\bar{b}$, $b\bar{b}Z$, $t\bar{t}t\bar{t}$ and single top.

$$\begin{aligned} S_T &> 0.1, \\ \Delta\phi &> 10 \text{ degrees}, \end{aligned}$$

where n_j is the number of jets (with $E_T > 50$ GeV and $|\eta_j| < 3.0$ as noted above). We display the $E_T^{\rm miss}$ distribution after these cuts (7) in Fig. 6 for the gluino signal benchmark point as well as for the various backgrounds. Unsurprisingly, S/B increases with $E_T^{\rm miss}$. As before, in the interest of preserving as much signal as possible, we choose a relatively conservative cut, keeping in mind that we can rely on other variables to further improve the signal to background ratio. Specifically we require the additional cut,

$$E_T^{\rm miss} > 1900 \text{ GeV}. \tag{8}$$

Next, we turn our attention to the E_T distributions of the leading jets. In Fig. 7 we display the distribution of the hardest jet E_T after cuts (7) and (8), based on which we implement the additional cut,

$$E_T(j_1) > 1300 \text{ GeV}. \tag{9}$$

We next show the distribution of the second leading jet E_T after the cuts (7 - 9) have been applied in Fig. 8. We impose the additional requirement,

$$E_T(j_2) > 900 \text{ GeV}. \tag{10}$$

We see that the signal, even for this rather heavy gluino benchmark point, dominates the background. Nevertheless, we checked the distributions of the third and fourth leading jets and

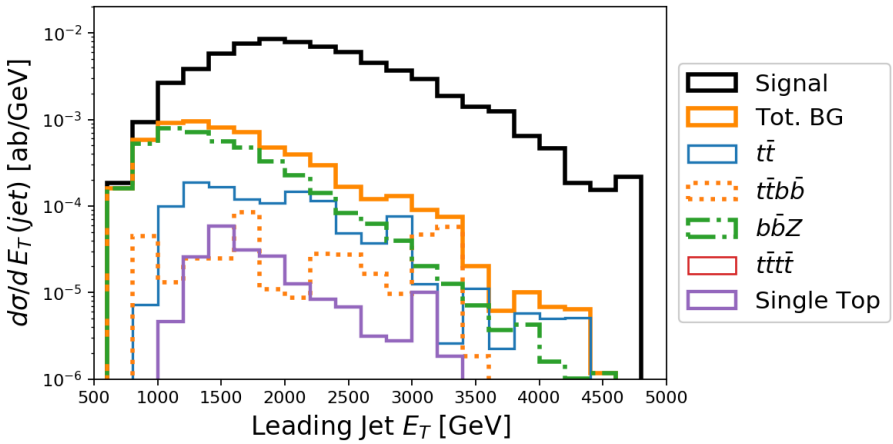

Figure 7: Distribution of leading jet E_T after initial cuts (7) and the subsequent harder $E_T^{\rm miss}$ cut (8) for the gluino signal as well as for the most relevant backgrounds.

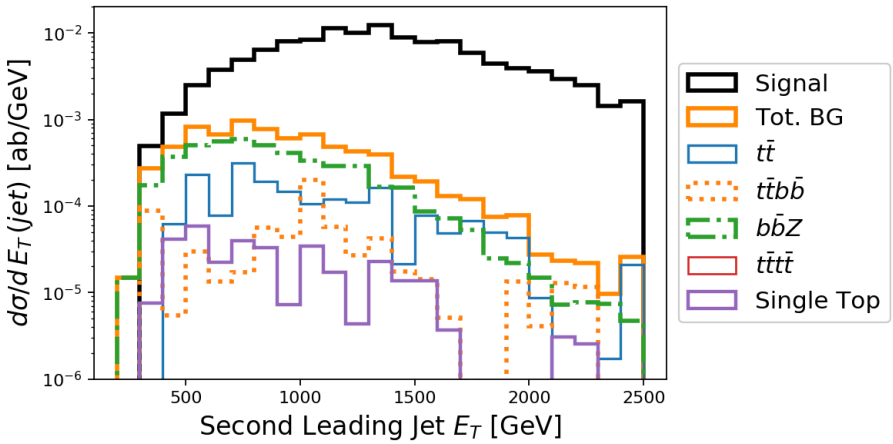

Figure 8: Distribution of second leading jet E_T after initial cuts (7), the subsequent harder $E_T^{\rm miss}$ cut (8), and the $E_T(j_1)$ cut (9) as well as for the most relevant backgrounds.

concluded that cuts on the E_T (or other properties) of these jets did not significantly help with the extraction of the signal. We do not display these distributions in the interests of brevity.

Thus, the cuts we use in our gluino discovery analysis at LHC33 are

$$\begin{aligned} n_b &\geq 2, \\ n_\ell &= 0, \\ E_T^{\rm miss} &> \max(1900\ {\rm GeV}, 0.2 M_{\rm eff}), \\ n_j &\geq 4 \\ E_T(j_1) &> 1300\ {\rm GeV}, \\ E_T(j_2) &> 900\ {\rm GeV}, \\ E_T(j_3) &> 200\ {\rm GeV}, \\ E_T(j_4) &> 200\ {\rm GeV}, \\ S_T &> 0.1, \\ \Delta\phi &> 10\ {\rm degrees}. \end{aligned} \tag{11}$$

After these cuts the total background cross section is 0.35 ab as compared to a signal cross section of 10.4 ab for the benchmark model. About 55% of this background arises from $b\bar{b}Z$ production, around 30% from $t\bar{t}$ production, and $\gtrsim 10\%$ from $t\bar{t}b\bar{b}$ production, with negligible contributions from other sources.

4 Stop and Gluino Reach at LHC33

We now use the optimized cuts designed in Sec. 3 to project discovery reaches and exclusion limits for stops and gluinos at LHC33. Our projections for stop reach, which are presented in Sec. 4.1, are in the context of the simplified model with light higginos used to develop the cuts. In establishing reach, we will vary the stop mass while leaving the higgsino masses fixed at around 150 GeV and take the branching fractions for the stop decays $\tilde{t}_1 \to t\widetilde{Z}_1, t\widetilde{Z}_2$ to be 25% each and the branching fraction for $\tilde{t}_1 \to b\widetilde{W}_1 = 50\%$ (as expected if the stop dominantly decays via Yukawa couplings). As we discussed earlier, this is representative of models with light higgsinos and relatively heavy gauginos. We fix the higgsino masses by choosing $\mu = 150$ GeV. We expect that our results are insensitive to the precise value as long as $m_{\tilde{t}_1} - m_t \gg |\mu|$.

The corresponding discovery contours and limits on the gluino mass are obtained in the context of the same simplified model, but (obviously) with the addition of a gluino, satisfying $m_{\tilde{g}} > m_{\tilde{t}_1}$. We expect this will capture the gluino reach in a wide variety of well-motivated light higgsino models where the gluino decays via $\tilde{g} \to t\tilde{t}_1$, with the stop decaying to higgsinos as detailed above.

4.1 Stop Reach

In Fig. 9, we show the stop pair production cross section after the stop analysis cuts (6). Specifically, we determine the efficiency with which stop signal events pass the analysis cuts for stop masses of 2250, 2500, 2750, 3000, 3250, 3500, and 4000 GeV and interpolate to find the

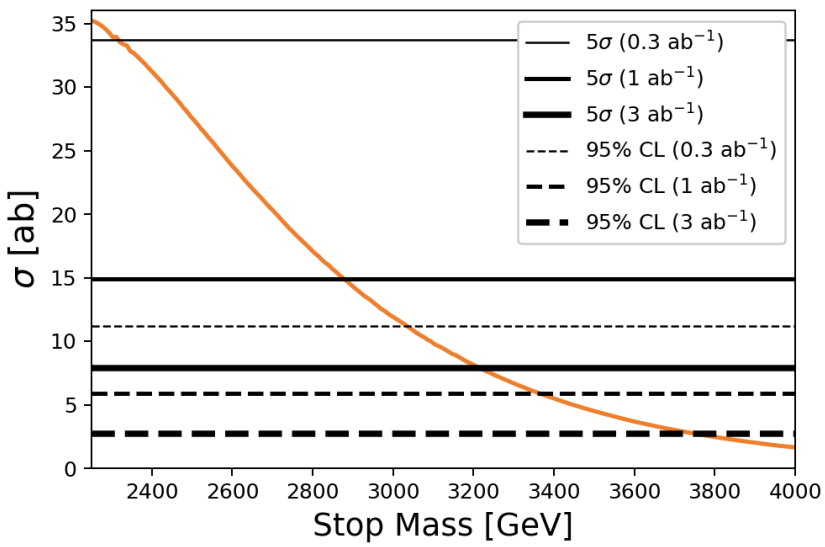

Figure 9: The stop signal cross section after the optimized analyses cuts (6) described in the text. The solid horizontal lines show the minimum cross section for which an upward Poisson fluctuation of the SM background, occurs with a Gaussian probability corresponding to 5σ, for integrated luminosities of 0.3, 1 and 3 ab^{-1} at LHC33. The dashed horizontal lines give the signal cross section which is excluded at 95% for the same choices of integrated luminosity.

efficiency for any stop mass. The total cross section comes from interpolating the NLO + NLL values from Ref. [31]. As in Sec. 3.1, we are considering only $pp \to \tilde{t}_1\tilde{t}_1^*$ production. We are assuming that the lightest two neutralinos and the lightest chargino are pure higgsinos with the masses given in Table 1 and that stops decay via $\tilde{t}_1 \to t\widetilde{Z}_1$, $\tilde{t}_1 \to t\widetilde{Z}_2$, and $\tilde{t}_1 \to b\widetilde{W}_1$ with branching fractions in the ratio $1:1:2$.

We calculate the signal cross section that will lead to an expected 5σ discovery as follows: (a) we take the expected number of signal plus background events to be the sum of signal and background cross sections, times the given luminosity, rounded to the nearest integer; (b) we find the value of signal cross section which gives an expected number of signal plus background events for which the Poisson probability of observing at least that many *background only* events is equal to the p-value that corresponds to 5σ, *i.e.*, $\approx 2.87 \times 10^{-7}$. The values of this quantity, *i.e.*, 33.7, 14.9, and 7.9 ab for 300 fb^{-1}, 1 ab^{-1}, and 3 ab^{-1}, respectively, are indicated by solid horizontal lines in Fig. 9. The discovery reach in this channel is then the value of the stop mass for which the signal cross section is equal to these discovery cross sections, *i.e.*, the values of stop mass at which the lighter/ orange cross section curves cross the discovery cross section lines. Specifically, we find that the 5σ mass reach for stop discovery in this channel is $m_{\tilde{t}_1} \approx 2300$, 2900, and 3200 GeV for 300 fb^{-1}, 1 ab^{-1}, and 3 ab^{-1}, respectively. We regard a signal as observable if we have a "5σ" significance together with least 5 signal events in the data sample and $S/B > 20\%$.

We also calculate the signal cross section which is expected to be ruled out at 95% confi-

dence level after various integrated luminosities. Specifically we find the expected number of background events, B, observed at the given luminosity by multiplying the background cross section by the integrated luminosity and rounding to the nearest integer. The signal expected to be ruled out at 95% confidence level is then the value of signal for which the Poisson probability of observing B or fewer events is 5%. The values of this quantity, *i.e.*, 11.2, 5.9, and 2.7 ab for 300 fb^{-1}, 1 ab^{-1}, and 3 ab^{-1} respectively, are indicated by dashed horizontal lines in Fig. 9; from this figure we see that the stop masses that we project would be excluded at 95% confidence level if no signal was observed are indicated by dashed horizontal lines in Fig. 9. From looking at the values of stop mass for which the cross section reaches these values, we find that the values of the stop mass expected to be ruled out at 95% are 3000, 3400, and 3800 GeV for 300 fb^{-1}, 1 ab^{-1}, and 3 ab^{-1} respectively[10].

These results have been obtained using the value of 4.6 ab for the background cross section obtained in Sec. 3.1. Especially since we are considering projections for a future machine and we are requiring two b-tagged jets in all of our analyses, one might wonder how our results would vary if we considered other parameterizations of the b-tagging efficiencies. Using the CMS "medium" b-tagging parameterization [28], the background cross section obtained from the analysis cuts (6) rises to 7.3 ab and under the CMS "tight" b-tagging parameterization this cross section falls to 1.8 ab. However, the signal cross section is affected in a similar way; using "medium" b-tagging the signal cross section for the benchmark 2.75 TeV stop point rises to 23.3 ab from the 18.9 ab we obtain with our default b-tagging parameterization (described in Sec. 2.1), so using the "medium" b-tagging parametrization would have minimal effects on our projections. Using the "tight" b-tagging parametrization reduces the signal cross section at this point to 5.6 ab. So our projections would change more substantially under this scenario, though re-optimizing our cuts with this b-tagging prescription would presumably lessen the changes. Finally, we note that even after scaling up our backgrounds by a factor of 10, we would still project 95% confidence level exclusions of stop masses below $\sim$ 3000 (3300) GeV with 1 (3) ab^{-1} of integrated luminosity.

4.2 Gluino Reach

The efficiency for gluino event detection, and hence the reach for discovery or exclusion in the gluino mass, also depends on the stop mass. For this reason, rather than only evaluating the reach along some particular model line, we examine the signal cross section in a simplified model identical to the one used for stop analyses in Secs. 3.1 and 4.1, except that now we also have a gluino, whose mass is an additional free parameter. We consider only gluino pair production, $pp \to \tilde{g}\tilde{g}$, where each gluino then decays via $\tilde{g} \to \tilde{t}_1\bar{t}$ or $\tilde{g} \to \tilde{t}_1^* t$ with 50% probability for each decay mode. The stop then decays to higgsinos via $\tilde{t}_1 \to t\widetilde{Z}_1$, $\tilde{t}_1 \to t\widetilde{Z}_2$, and $\tilde{t}_1 \to b\widetilde{W}_1$ in the ratio 1 : 1 : 2.

[10]The reader may wonder whether the stop reach would be significantly enhanced if the lighter stop was mainly left-handed so that the signal also receives comparable contributions from sbottom pair production. We view a significant increase in the signal rate to be unlikely in high scale models because even if the LL diagonal elements of the stop and sbottom squared mass matrices are comparable, the much larger off-diagonal element of the stop mass squared matrix will tend to depress the mass of $\tilde{t}_1$ to be well-below that of $\tilde{b}_1$. The reader may view the reach projection in the figure as erring on the conservative side.

We determine the efficiency with which generated events pass the analysis cuts for a number of simplified model points in the $m_{\tilde{g}} - m_{\tilde{t}_1}$ plane and interpolate. In performing this interpolation, we take the efficiency to go to zero when $m_{\tilde{t}_1} + m_t = m_{\tilde{g}}$. This is unduly conservative: as we will see below, there is considerable sensitivity where the gluino decays via off-shell stops, but these decay modes are not a part of our simplified model.

We then multiply our interpolation of efficiency by an interpolation of the NLO + NLL gluino cross section [31]. The final cross sections after the analysis cuts (11), for different choices of stop mass, are shown in Fig. 10. As in Fig. 9, the horizontal solid lines represent the signal cross sections for which we would expect a 5σ discovery for the given values of integrated luminosity, and the horizontal dashed lines represent the signal cross section expected to be excluded at 95% confidence level, where these values have been calculated by the same procedure as in Sec. 4.1. We see that with 1 ab^{-1} the discovery reach in the gluino mass ranges from just over 5 TeV (if the stop is light enough to be discovered even at the 14 TeV LHC) to around 5.6 TeV; with 3 ab^{-1} the discovery reach is over 6 TeV for larger values of the stop mass. Along the model line with radiatively-driven naturalness (RNS) studied in Ref. [13], the gluino mass discovery reach is 5380 GeV with 1 ab^{-1} and 5930 GeV with 3 ab^{-1}, to be compared with $\sim$ 2640 GeV and 2800 GeV at the HL-LHC. As in the case of the stop analyses, using the CMS medium b-tagging prescription raises both signal and background cross sections, while using the tight prescription will reduce these cross sections. In neither case would results be qualitatively changed, and, if we were to re-optimize cuts for a different b-tagging prescription, the overall impact on the reach would be rather small.

The simplified models we have used to obtain the above projections clearly do not cover all the possibilities. The first other possibility is that we have a gluino mass below $m_{\tilde{t}_1} + m_t$. Provided the light stop (and possibly the light sbottom) mass are much lighter than the first and second generation squarks, the gluino will decay to a third generation quark, a third generation antiquark, and a higgsino. The specific branching ratios depend on the mass of the light stop and sbottom as well as, *e.g.*, the $\tilde{t}_L$ component of the light stop. We, therefore, consider two additional simplified models to cover such a possibility. In one, the lightest stop is purely the right-handed stop with mass $m_{\tilde{t}_1} = 2m_{\tilde{g}}$ and the light sbottom as well as the heavier stop are decoupled. In the other, the light stop and sbottom are both purely left-handed, and $m_{\tilde{b}_1} \simeq m_{\tilde{t}_1} = 2m_{\tilde{g}}$. The discovery reach and exclusion projections for these two simplified models are shown in Fig. 11. We note that the discovery and exclusion reaches in these scenarios are (a) very similar to each other and (b) similar to the discovery and exclusion reaches in the simplified model scenario considered above. In particular the 1 (3) ab^{-1} 5σ discovery reach in these simplified models is $\approx$ 5510 (6070) GeV. We conclude that our gluino reach results are only weakly dependent on the third generation squark mass as long as we are not extremely close to the kinematic boundary for two-body gluino decays.

The last possibility for decoupled first/second generation squarks is that $m_{\tilde{g}} > m_{\tilde{t}_1} + m_t$, but the gluino also decays to other third generation squarks, such as $\tilde{t}_2$. It is clearly more difficult to definitively probe this scenario in generality, but we note that if additional light stops or sbottoms play a prominent role in the most important decay chains, as we would generally expect, then we would still expect to be able to observe such models with the cuts given above with comparable efficiency, so our reach results would not be qualitatively altered.

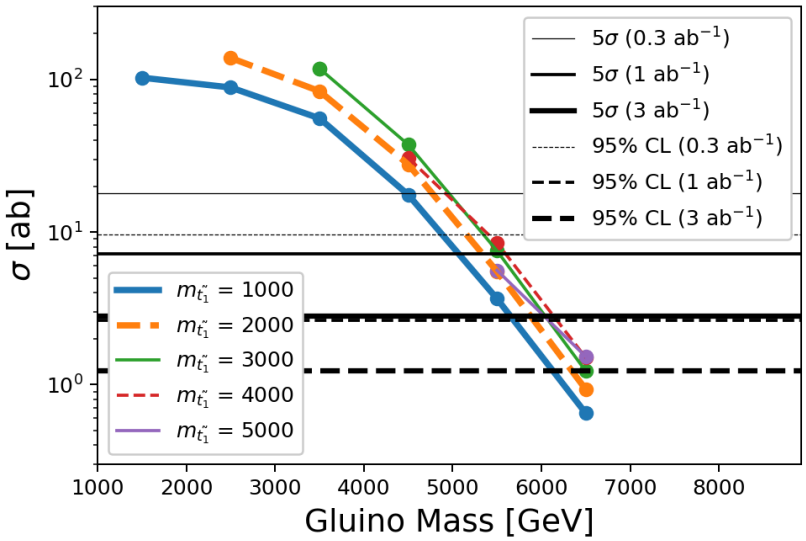

Figure 10: The gluino signal cross section for the optimized analyses cuts (11) described in the text for various choices of stop mass. The solid horizontal lines show the minimum cross section for which an upward Poisson fluctuation of the SM background, for which the cross section is 0.35 ab, occurs with a Gaussian probability corresponding to 5σ for integrated luminosities of 0.3, 1, and 3 ab^{-1} at LHC33. The dashed horizontal lines give the signal cross section which is excluded at 95% for these same values of integrated luminosity.

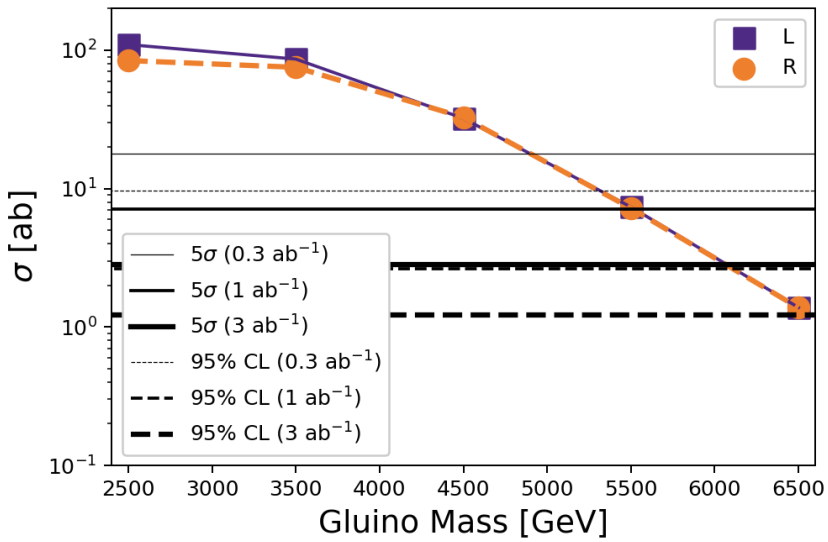

Figure 11: The gluino signal cross section for the optimized analyses cuts (11) for the two additional simplified models in which the gluino decays via three-body decays mediated by $\tilde{t}_R$ or by the left-handed third generation squark doublet as described in the text. The solid horizontal lines show the minimum cross section for which an upward Poisson fluctuation of the SM background, for which the cross section is 0.35 ab, occurs with a Gaussian probability corresponding to 5σ for integrated luminosities of 0.3, 1, and 3 ab^{-1} at LHC33. The dashed horizontal lines give the signal cross section which is excluded at 95% for several values of integrated luminosity.

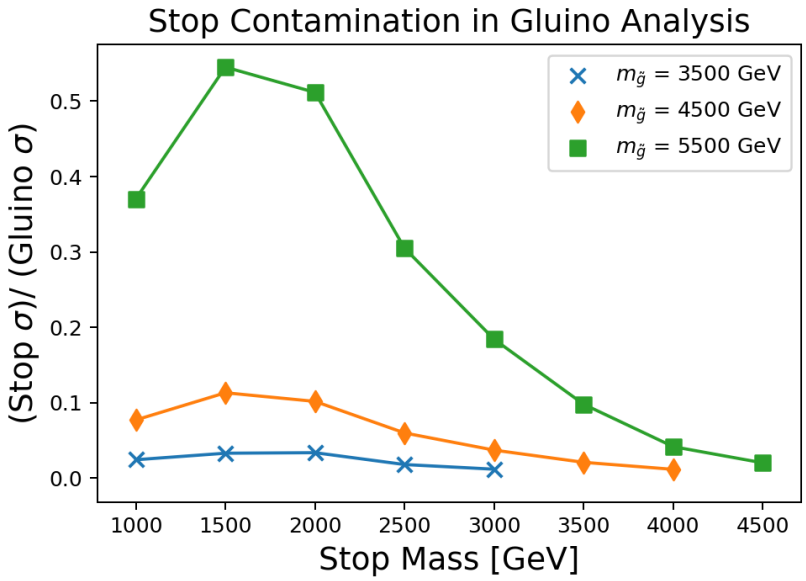

Figure 12: The ratio of (i) the cross section for (contamination from) stop pair production events at LHC33 the passing the gluino analysis cuts (11) to (ii) the corresponding cross section for signal events from gluino pair production, with subsequent gluino decays to $\tilde{t}_1\bar{t}$ or $\tilde{t}_1^* t$, passing the gluino analysis cuts, versus $m_{\tilde{t}_1}$, for three values of the signal gluino mass.

4.3 Distinguishing Stops from Gluinos

Up to this point our focus has been on the discovery of *new physics* due to the production of stops or gluinos at LHC33: *i.e.*, in our projections of the stop and gluino reaches, we have only been concerned whether the SUSY signal can be detected above various SM backgrounds, regardless of its origin. In this section, we examine whether the observation of a signal via either the stop or the gluino search strategy enables us to unequivocally claim the discovery of the corresponding particle (assuming a SUSY origin of the signal) or whether contamination between channels can lead us to incorrect inferences.

Toward this end, in Fig. 12, we show the ratio of the cross section from stop production (contamination) and that for the gluino signal, after the gluino analysis cuts (11). We illustrate this ratio as a function of $m_{\tilde{t}_1}$ for three representative values of the signal gluino mass. We see that the stop contamination, though considerably larger than the SM background of 0.35 ab, is significantly smaller than the gluino signal, except for values of $m_{\tilde{g}}$ approaching the LHC33 reach. The contamination falls off not only for very heavy stops, for which the production is kinematically suppressed, but also for relatively light stops because stop events then have a very low efficiency for passing the gluino cuts.

The opposite situation – contamination of the stop signal from gluino production events – is illustrated in Fig. 13 as a function of $m_{\tilde{g}}$. We see that the situation is quite different in that, unless the gluino is very heavy, the stop sample is typically dominated by gluino production events. This should not be surprising because gluino pair production, which has a

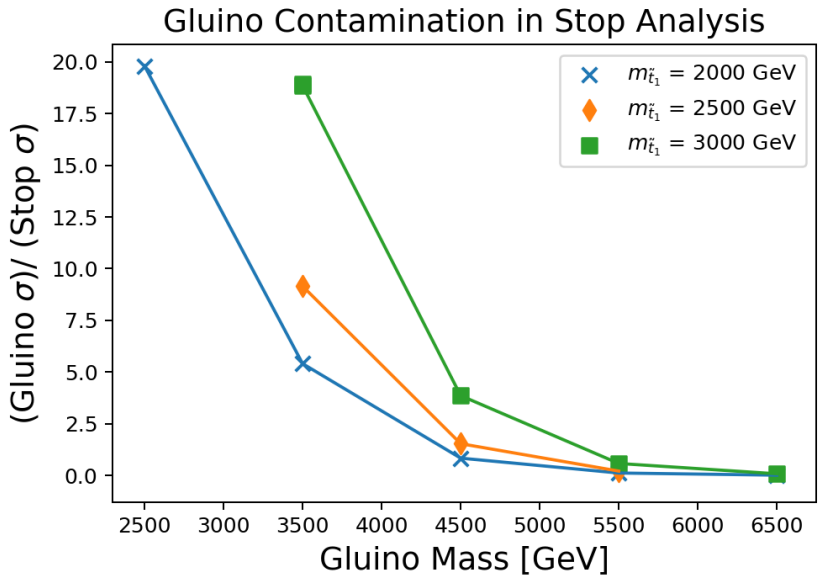

Figure 13: The ratio of (i) the cross section for (contamination from) gluino pair production, with subsequent gluino decays to $\tilde{t}_1\bar{t}$ or $\tilde{t}_1^* t$, for LHC33 events passing the stop analysis cuts (6) to (ii) the corresponding cross section for signal events from stop pair production passing the same analysis cuts, versus $m_{\tilde{g}}$, for three values of the signal stop mass.

much higher cross section, also results in the production of stop pairs. Since gluino production can contaminate the stop sample with a large rate, it is clear that a discovery of new physics via the stop selection cuts (6) would not unequivocally signal direct stop pair production, even if we assume the new physics has a SUSY origin [40].

Before turning to the examination of whether stop and gluino pair production mechanisms can be disentangled from one another, we stress that the contamination of the stop sample by gluino events, or *vice-versa*, does not negatively affect the extraction of the new physics reach that we have discussed in the last section. If anything, this reach will be enhanced because events from gluino production will also contribute to the signal in the stop analysis, and, to a much smaller degree, the other way around.

Turning to an examination of different ways to determine whether a SUSY signal arises from gluino or direct stop pair production, we note that gluino events contain two additional hard tops in addition to the stop pair. Thus, (a) we expect the b-multiplicity to be greater in the gluino pair production case, and (b) we typically expect additional *very hard jets* (and perhaps also leptons) in the gluino pair production case. To illustrate these differences, we consider a simplified model point with a gluino mass of 4.5 TeV and a stop mass of 2 TeV. We show the tagged b-jet multiplicity distribution for events which pass the stop [gluino] selection cuts (6) [(11)] in Fig. 14 as the dashed [solid] histograms. Distributions from stop production are shown by lighter/ orange histograms, while those from gluino production are shown by the darker/ purple histograms. We see that events with $n_b \geq 3$, which constitute about 10 - 15% (which would require ab^{-1} scale integrated luminosities for observable rates depending on $m_{\tilde{g}}$)

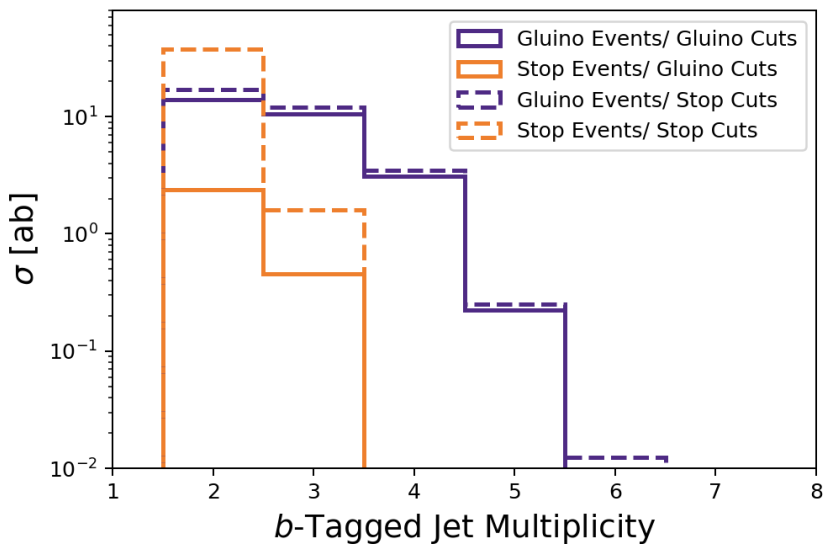

Figure 14: The distribution of multiplicity of tagged b-jets in events from gluino pair production (darker/ purple) and from stop pair production (lighter/ orange) in a simplified model with $m_{\tilde{g}} = 4.5$ TeV and $m_{\tilde{t}_1} = 2$ TeV after the stop analysis cuts (dashed histogram) (6) and after the gluino analysis cuts (solid histogram) (11).

of the gluino sample, can only come from gluino production.

We show the jet multiplicity distribution for jets with $E_T > 600$ GeV in Fig. 15.[11] We see that, after the stop selection cuts, the bulk of stop events have just two very hard jets, while exactly the reverse is true for gluino events. Indeed, we see that this distribution serves to separate the gluino and stop production mechanisms, except perhaps in the case that $m_{\tilde{g}}$ is unfortunately close to $m_{\tilde{t}_1}$.

Unless $m_{\tilde{t}_1}$ is relatively close to $m_{\tilde{g}}$, further separation between gluino and stop production events may be possible using kinematic distributions such as the $M_{\rm eff} \equiv E_T(j_1) + E_T(j_2) + E_3(j_3) + E_T(j_4) + E_T^{\rm miss}$ distribution shown in Fig. 16, or the third jet E_T distribution shown in Fig. 17. However, if the gluino is just a little heavier than the stop, it is possible that these distributions may merge, and it may be difficult to unequivocally tell whether we have stop pair production in addition to the large gluino signal. Even in this difficult case, progress may be possible. For instance, it should be possible to extract the gluino signal and determine its mass from the total rate for gluino events as proposed in Ref. [13] (the stop contamination is completely negligible in such a case). This can then be used to project gluino contamination in the stop sample, enriched using additional hard jet multiplicity and n_b cuts. A detailed study

[11] We have checked that though the jet multiplicity distributions (with jets being defined as 50 GeV hadronic clusters) from stop and gluino pair production are also reasonably separated, these are not as distinct as the multiplicity distributions of just the very hard jets shown in Fig. 15, in part because of radiated QCD jets, and perhaps also because decay products of very boosted higgsinos can sometimes form a 50 GeV jet. By focussing on hard jets, we are more likely to count the jets only from the primary decays of the stops/gluinos.

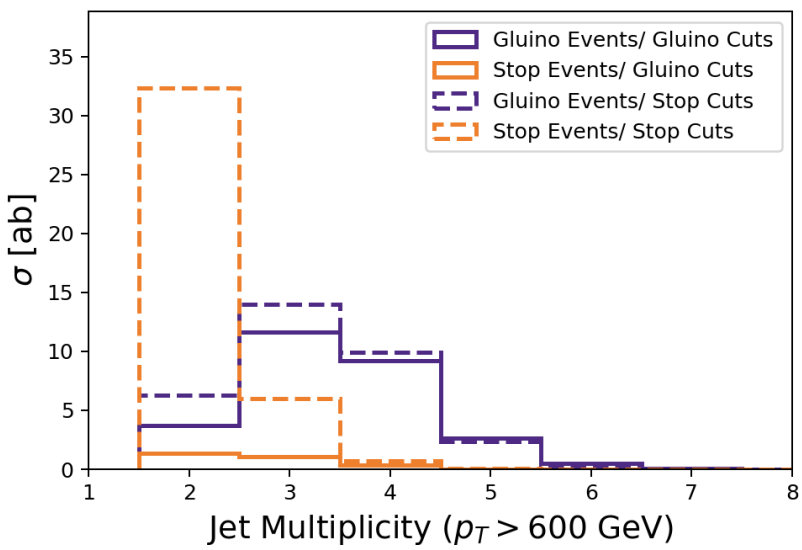

Figure 15: The distribution of jet multiplicity for jets with $E_{Tj} > 600$ GeV in events from gluino pair production (darker/ purple) and from stop pair production (lighter/ orange) in a simplified model with $m_{\tilde{g}} = 4.5$ TeV and $m_{\tilde{t}_1} = 2$ TeV after the stop analysis cuts (dashed histogram) (6) and after the gluino analysis cuts (solid histogram) (11).

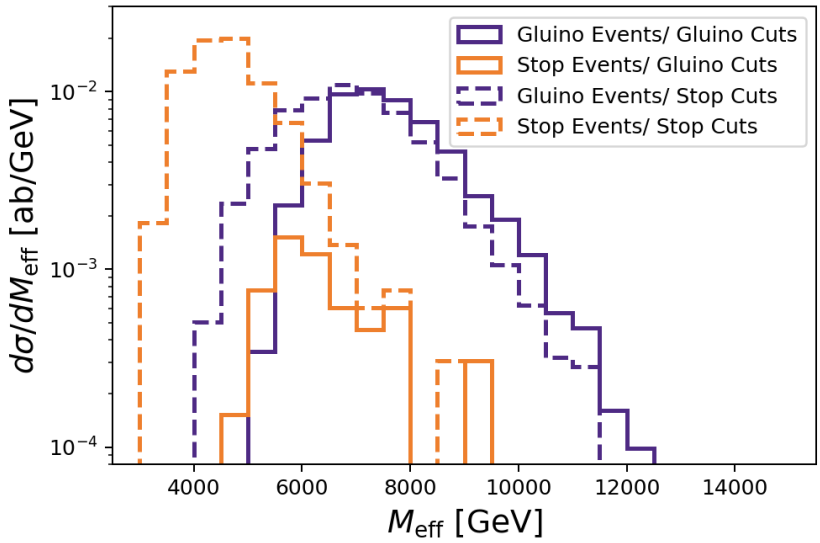

Figure 16: The distribution of $M_{\rm eff}$ in events from gluino pair production (darker/ purple) and from stop pair production (lighter/ orange) in a simplified model with $m_{\tilde{g}} = 4.5$ TeV and $m_{\tilde{t}_1} = 2$ TeV after the stop analysis cuts (dashed histogram) (6) and after the gluino analysis cuts (solid histogram) (11).

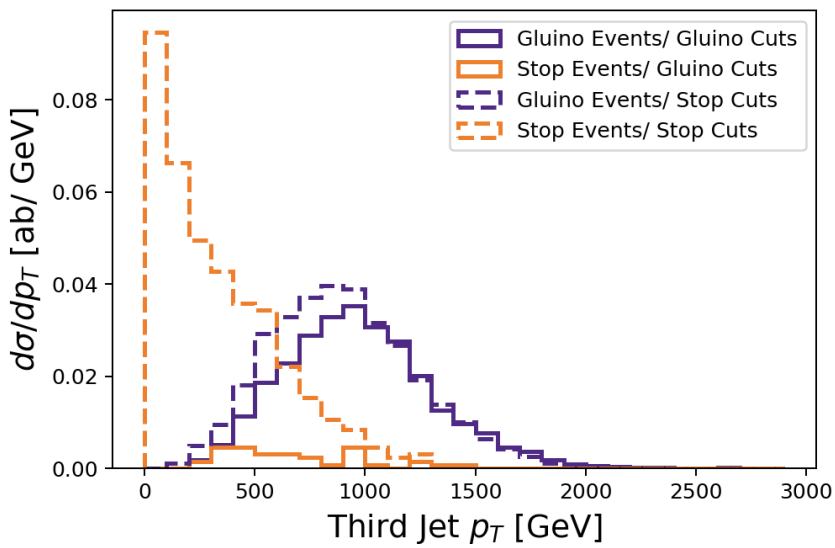

Figure 17: The distribution of multiplicity of $E_T(j_3)$ in events from gluino pair production (darker/ purple) and from stop pair production (lighter/ orange) in a simplified model with $m_{\tilde{g}} = 4.5$ TeV and $m_{\tilde{t}_1} = 2$ TeV after the stop analysis cuts (dashed histogram) (6) and after the gluino analysis cuts (solid histogram) (11).

of this is beyond the scope of the present analysis.

5 Implications of LHC33 Reach Results for Natural SUSY Models

We have just seen that in models with light higgsinos, experiments at LHC33 should be able to discover stops with masses up to $2.8 - 3.2$ TeV and gluinos out to $\sim 5.5 - 6.0$ TeV, assuming that gluinos dominantly decay via $\tilde{g} \to \tilde{t}_1 t$ (or via three-body decays to third generation quarks and higgsinos). In this section, we focus on the implications of these results for natural SUSY models that have received much attention over the last several years.

Many authors have argued that SUSY naturalness requires light stops, with masses ranging from a few hundred GeV to around 1 TeV, depending on the degree of fine-tuning that is allowed. It has also been suggested that the current LHC lower limits on stop masses are already in tension with naturalness. Implicit in this reasoning is the unstated assumption that the underlying model parameters are independent. The arguments that lead to these strong bounds on stop masses do not apply if the underlying model parameters are correlated, as will almost certainly be the case once the underlying SUSY-breaking mechanism is understood. Here, we adopt a more conservative approach to fine-tuning [18, 19] which recognizes the possibility that model parameters (usually taken to be independent) might be correlated in the underlying theory.

Toward this end, we begin with the well-known expression that yields the measured value of m_Z in terms of the weak scale SUSY Lagrangian parameters,

$$\frac{m_Z^2}{2} = \frac{m_{H_d}^2 + \Sigma_d^d - (m_{H_u}^2 + \Sigma_u^u)\tan^2\beta}{\tan^2\beta - 1} - \mu^2 \simeq -m_{H_u}^2 - \Sigma_u^u - \mu^2, \tag{12}$$

where the last equality is valid for moderate to large values of $\tan\beta$. The quantities Σ_u^u and Σ_d^d in Eq. (12) arise from 1-loop corrections to the scalar potential (their forms are listed in the Appendix of Ref. [19]), $m_{H_u}^2$ and $m_{H_d}^2$ are the soft SUSY-breaking Higgs mass parameters, $\tan\beta \equiv \langle H_u\rangle/\langle H_d\rangle$ is the ratio of the Higgs field VEVs, and μ is the superpotential (SUSY conserving) Higgs/higgsino mass parameter. SUSY models requiring large cancellations between the various terms on the right hand side of Eq. (12) to reproduce the measured value of m_Z^2 are regarded as fine-tuned. With this in mind, we adopt the *electroweak* fine-tuning measure, $\Delta_{\rm EW}$, which compares the maximum absolute value of each term on the right-hand-side of Eq. (12) to the left-hand-side, $m_Z^2/2$.

The electroweak fine-tuning parameter yields the minimal fine-tuning for a given sparticle spectrum. We advocate its use for discussions of fine-tuning because it allows for the possibility that SUSY-breaking parameters (frequently assumed to be independent in the evaluation of fine-tuning) might be correlated in the underlying SUSY theory. Moreover, as we have previously argued, the traditionally used fine-tuning measure, $\Delta_{\rm BG}$ [41], reduces to $\Delta_{\rm EW}$ once correlations between parameters are correctly incorporated [42]. We stress that $\Delta_{\rm BG}$, computed without parameter correlations being implemented, could easily be two orders of magnitude larger than $\Delta_{\rm EW}$. For this reason, discarding models as unnatural because $\Delta_{\rm BG}$ (computed naively) is $\sim 100-1000$ could exclude perfectly viable underlying theories. In this paper, we conservatively adopt $\Delta_{\rm EW} < 30$ (corresponding to no more than a part in thirty electroweak fine-tuning) as a criterion for naturalness of the superpartner spectrum. The onset of electroweak fine-tuning for values $\Delta_{\rm EW} \gtrsim 20-30$ is visually displayed in Refs. [43] and [44].

5.1 Radiatively-driven Natural SUSY (RNS)

We see from Eq. (12) that in order to obtain low values of $\Delta_{\rm EW}$, the weak scale values of $m_{H_u}^2$ and μ^2 must both have magnitudes not much larger than m_Z^2. At the same time, LHC search constraints seem to require at least TeV-scale high scale soft terms. These two facts can be reconciled in models with radiatively-driven naturalness (radiative natural SUSY or RNS) wherein a large GUT scale value of $m_{H_u}^2$ is driven to small weak scale values via renormalization group running. In the focus point region of the mSUGRA/CMSSM model, $m_{H_u}^2$ is indeed driven to small negative values. However, the FP region is mainly viable for small A_0 values while the rather large Higgs mass $m_h \simeq 125$ GeV requires large mixing from large A terms. The main obstacle in the mSUGRA/CMSSM model to having both naturalness and $m_h \simeq 125$ GeV arises from the rather unmotivated assumption of scalar mass universality, $m_{H_u} = m_{H_d} = m_0$, at the GUT scale. Such universality is not expected to occur in SUSY GUT models since the Higgs multiplets live in different GUT representations than the matter multiplets.

This led us to exmine the two-extra-parameter non-universal Higgs model [45] with $m_{H_u} \neq m_{H_d} \neq m_0$ always allows the freedom to adjust $m_{H_u}^2$(GUT) to whatever value is needed such

that it is driven to small negative values at the weak scale.[12] In NUHM2, the independent GUT scale values of $m_{H_u}^2$ and $m_{H_d}^2$ can be traded for weak scale values of μ and m_A so that a natural value of $\mu \sim 100 - 300$ GeV can always be chosen. Then Eq. (12) can be used to determine the weak scale value of $m_{H_u}^2$ which is then driven via RGEs to determine $m_{H_u}^2$(GUT). Thus, in NUHM2 (and other SUSY models which allow for high-scale freedom in the Higgs soft terms), electroweak naturalness, *i.e.*, $\Delta_{\rm EW} < 30$, can be satisfied if the high scale μ-parameter, which typically does not evolve very much, is selected to be $\sim m_{weak}$ and the Σ_u^u terms are not too large.

The most robust feature of RNS models is that these include four light higgsinos-like states $\widetilde{Z}_1, \widetilde{Z}_2, \widetilde{W}_1^{\pm}$ with masses $\sim 100 - 300$ GeV because the weak scale value of μ^2 directly enters Eq. (12).[13] If bino and wino mass parameters are large (which is typically the case in models with gaugino mass unification which obey LHC gluino mass constraints), the mass splitting between the higgsinos is small, so the visible decay products of $\widetilde{Z}_2$ and $\widetilde{W}_1^{\pm}$ are very soft so that signals from electroweak higgsino pair production are typically buried below SM backgrounds at the LHC. We should mention that electroweak naturalness also imposes upper bounds on stop and gluino masses in the RNS framework. The bounds on stop masses arise because these produce large corrections to the Higgs effective potential and are manifested by large contributions to Σ_u^u in Eq. (12). A low value of $\Delta_{\rm EW}$ requires a large SUSY-breaking trilinear stop parameter comparable to the (third generation) scalar mass parameter. This simultaneously leads to sizeable left-right stop mixing and automatically lifts the light Higgs boson mass to its observed value [18]. The upper limit on $m_{\tilde{g}}$ arises because heavy gluinos result in large radiative corrections to the stop masses [49]. We will return to these stop and gluino limits, which are (only weakly) sensitive to the details of the underlying RNS model, later in this section.

5.1.1 The natural NUHM2 model

The NUHM2 model, with two additional parameters $m_{H_u}^2$(GUT) and $m_{H_d}^2$(GUT) *vis-à-vis* the mSUGRA/CMSSM model, is the prototypical RNS model. One special feature of this NUHM2 RNS model is the assumed gaugino mass unification which constrains the wino mass to be $\sim m_{\tilde{g}}/3$ and the bino mass to be $\sim m_{\tilde{g}}/6$. This has two important consequences:

1. As the integrated luminosity accumulated at the LHC increases, it has been shown that wino pair production provides a deeper reach into parameter space than gluino pair production. Wino pair production leads to clean same-sign dilepton events free from jet activity (other than that from QCD radiation) via same sign diboson (SSdB) production processes [14] arising from $pp \to \widetilde{W}_2^{\pm}\widetilde{Z}_4$ with $\widetilde{W}_2^{\pm} \to W^{\pm}\widetilde{Z}_{1,2}$ and $\widetilde{Z}_4 \to W^{\pm}\widetilde{W}_1^{\mp}$. Since

[12] A common objection is that then the high scale value of $m_{H_u}^2$ must be tuned just right to be driven to small negative values. However, if the proper correlations amongst soft terms are present, then a generalized focus point mechanism operates such that a large range of $m_{H_u}^2$ values are all focussed to small negative values at the weak scale: see Ref. [46].

[13] Here, we implicitly assume that the superpotential parameter, μ, is the dominant source of the higgsino mass. A soft SUSY-breaking contribution to the higgsino mass is possible if there are no additional gauge singlets that couple to higgsinos [47]. There are also extended frameworks with additional TeV scale fields that show it is theoretically possible to decouple the higgsino mass from the Higgs boson mass parameter that enters into Eq. (12) [48].

the naturalness upper limit on $m_{\tilde{g}}$ also implies a corresponding upper limit on the wino mass, this clean signal channel leads to a HL-LHC (3000 fb^{-1}) reach to $m_{1/2} \sim 1.2$ TeV, covering nearly all of the $\Delta_{\rm EW} < 30$ region consistent with the observed value of Higgs boson mass.

2. In the NUHM2 RNS model, the fact that the wino and bino masses are bounded above implies that higgsino mass gap, $m_{\widetilde{Z}_2} - m_{\widetilde{Z}_1}$, though small, is always larger than ~ 10 GeV over the entire range of parameters with $\Delta_{\rm EW} < 30$. Although electroweak production of higgsinos is swamped by SM backgrounds due to the small visible energy release in higgsino decays, higgsino pair production in association with a hard QCD jet– for instance $pp \to \widetilde{Z}_1\widetilde{Z}_2 + jet$ or $\widetilde{W}_1\widetilde{Z}_2 + jet$ with $\widetilde{Z}_2 \to \widetilde{Z}_1\ell^+\ell^-$– offers a HL-LHC reach to $\mu \sim 250$ GeV [50]. The detectability of the soft dilepton pair with $m_{\ell\ell} < m_{\widetilde{Z}_2} - m_{\widetilde{Z}_1}$, which is very sensitive to the size of the neutralino mass gap, plays a critical role in limiting the SM background.

A combination of these two signals covers essentially the entire parameter space of the natural NUHM2 model with $\Delta_{\rm EW} < 30$ at the HL-LHC. Unfortunately, this cannot be said to cover all natural SUSY models since the assumption of gaugino mass unification, which played a critical role in our discussion, can be relaxed without affecting naturalness. We are thus led to examine other well-motivated natural SUSY models where gaugino masses do not unify at $Q = M_{\rm GUT}$, and where weak scale wino and bino mass parameters are closer to the gluino mass.

5.1.2 The natural NUHM3 model

The natural NUHM3 model is an obvious extension of the natural NUHM2 model where we allow the high scale third generation mass, $m_0(3)$, to be independent of the first and second generation scalar masses. Gaugino mass parameters are assumed to be unified at $Q = M_{\rm GUT}$. This framework is partly motivated because it allows very heavy first and second generation squarks – which ameliorates the SUSY flavor problem – while keeping the third generation in the TeV range which is consistent with naturalness considerations. From the theory side, it is worth noting that there are extra-dimensional top-down models where the third generation feels SUSY breaking differently from the first two generations because of the geography of extra dimensions; see Sec. 5.1.4 below. As discussed in Sec. 5.2, the important point is that this additional freedom allows considerably heavier gluinos than the NUHM2 RNS model.

5.1.3 Natural Generalized Mirage Mediation (nGMM)

The mirage mediation (MM) framework [51] is a well-motivated top-down model that emerges from string theory where moduli fields are stabilized via flux compactification. Within this framework, the soft SUSY-breaking parameters typically receive comparable contributions from moduli-mediated and anomaly-mediated contributions to SUSY breaking. As a result, the superpartner spectrum is qualitatively different from that obtained in supergravity models. Since it was first proposed over a decade ago [52], it has been shown that the scalar masses and A-parameters are sensitive to the details of moduli stabilization and potential uplifting

mechanisms, while the gaugino mass pattern is robust [53] with gaugino masses being given by

$$M_a = \frac{m_{3/2}}{16\pi^2}\left(\alpha + b_a g_a^2\right). \tag{13}$$

Here $m_{3/2}$ is the gravitino mass, and the phenomenological parameter α measures the relative strengths of the moduli- and anomaly-mediated contributions to the gaugino masses. The hallmark of MM models is that the measured values of gaugino masses should apparently unify at the scale

$$\mu_{\rm mir} = M_{\rm GUT} \exp^{\frac{-8\pi^2}{\alpha}},$$

while the gauge couplings unify, as usual, at $M_{\rm GUT}$. There is no physical threshold at the scale $\mu_{\rm mir}$, which has led to this mixed-modulus anomaly-mediation framework being dubbed "mirage unification". If $\mu_{\rm mir}$ is close to the weak scale, the gaugino mass spectrum will be very compressed, giving rise to a well-motivated top-down framework where winos (and binos) can be essentially as heavy as gluinos.[14]

It has been shown that the original MM models where scalar masses are determined from specific values of modular weights are very fine-tuned over the entire range of parameters consistent with LHC sparticle and Higgs mass constraints [54]. In more general constructions, it was found that scalar masses and SUSY-breaking trilinear soft parameters are sensitive to the details of the moduli stabilization and potential uplifting mechanisms, while gaugino masses remain as in Eq. 13. These considerations led us to propose a phenomenological generalization of the MM framework, hereafter referred to as Generalized Mirage Mediation (GMM), where scalar mass and trilinear soft terms are determined by continuous rather than discrete parameters, but where gaugino masses are still given by Eq. (13). We refer the interested reader to Ref. [55] for detailed expressions for the GMM soft term values. The parameter freedom of the GMM model allows for superpartner mass values yielding $\Delta_{\rm EW}$ as low as ~ 15 with $m_h \simeq 125$ GeV, but with much heavier bino and wino masses (for a given value of $m_{\tilde g}$) as compared to models (such as NUHM2) with gaugino mass unification. Thus, in natural GMM, the SSdB signal as well as the monojet plus soft dilepton signal (discussed in Sec. 5.1.1) can become potentially unobservable even at the HL-LHC. In such a case, natural SUSY may well elude the scrutiny of HL-LHC; discovery of SUSY will then require new facilities. The GMM model has been incorporated into the Isajet/Isasugra computer code [56] which we use here to evaluate the superpartner spectrum as well as for calculations of electroweak fine-tuning.

5.1.4 The Natural Mini-Landscape

The mini-landscape program is an attempt to target special regions of the landscape of heterotic string theory (which allows for localized grand unification) where the effective low energy theory is the MSSM [57]. Detailed exploration in a series of papers has led to a picture of the emergent 4-D theory whose properties are determined by the geometry of the compact manifold and the location of the matter and Higgs (super)fields on this manifold. The gauge group is $SU(3)_{\rm col} \times SU(2)_L \times U(1)_Y$, though this symmetry may be enhanced for fields confined to fixed points

[14] If the auxiliary field whose vacuum expectation value breaks SUSY transforms as a **75** dimensional representation rather than a singlet of $SU(5)$, the weak scale gaugino masses have the ratio $M_1 : M_2 : M_3 = 6, 6, -5$, also resulting in a very compressed gaugino spectrum.

or fixed tori in the compactified dimensions. Examination of models has led to the following general picture [58].

1. The first two generations of matter live on orbifold fixed points and exhibit a larger $SO(10)$ gauge symmetry with first and second generation (s)fermions filling out the 16-dimensional spinor representation of $SO(10)$.

2. The Higgs multiplets, H_u and H_d, live in the untwisted sector and are bulk fields that feel just $G_{\rm SM}$. These fields, as well as the gauge multiplets, come in incomplete GUT multiplets, automatically resolving the doublet-triplet splitting problem.

3. The third generation quark doublet and the top singlet also reside in the bulk and thus have large overlap with the Higgs fields and correspondingly large Yukawa couplings. The small overlap of Higgs and first and second generation fields (which do not extend into the bulk) accounts for their much smaller Yukawa couplings. The location of other third generation matter fields is model-dependent. For simplicity, we assume that they also to live in the bulk.

4. Supergravity breaking may arise from hidden sector gaugino condensation with $m_{3/2} \sim \Lambda^3/m_{\rm Pl}^2$, with the gaugino condensation scale $\Lambda \sim 10^{13}$ GeV. SUSY breaking effects are felt differently by the various MSSM fields, depending on their location. The Higgs and stop fields in the untwisted sector feel extended supersymmetry (at tree level) in 4-dimensions, and are thus more protected than the fields on orbifold fixed points which receive protection from just $N = 1$ supersymmetry [59]. First and second generation matter scalars are thus expected with masses $\sim m_{3/2} \sim 10 - 30$ TeV. Third generation and Higgs soft mass parameters (which enjoy the added protection from extended SUSY) are suppressed by an additional loop factor $\sim 4\pi^2 \sim \log(m_{\rm Pl}/m_{3/2})$ typically expected in MM models. Gaugino masses and third generation trilinear soft terms are suppressed by the same factor, leading to TeV-scale mass values as expected from the nGMM framework discussed above. The main difference is that while all matter field generations were assumed comparable in the GMM framework, the mini-landscape picture distinguishes the third generation from the much heavier first two generations.

Several aspects of the spectrum of these models are qualitatively similar to that of the GMM models. The main difference is that while the three generations of matter scalars are treated identically in the GMM framework (except, of course, for the difference in Yukawa interactions); in the mini-landscape picture, the first and second generation sfermions are considerably heavier than their third generation cousins. In this sense, the natural mini-landscape picture is closer to the NUHM3 RNS model, but differs from it because the gaugino mass pattern is determined by MM rather than by gaugino mass unification. The broad brush phenomenology of the natural mini-landscape picture has been laid out in Ref. [60], to which we refer the reader for details. We have used Isajet/Isasugra [56] for the evaluation of the superpartner spectrum, as well as for $\Delta_{\rm EW}$, in this framework. For our purposes, the gaugino spectrum is compressed for viable regions of model parameter space, so that, as in the nGMM model, the SSdB and monojet plus soft dilepton signals may be inaccessible, and we may have to rely on gluino and stop signals for definitive detection.

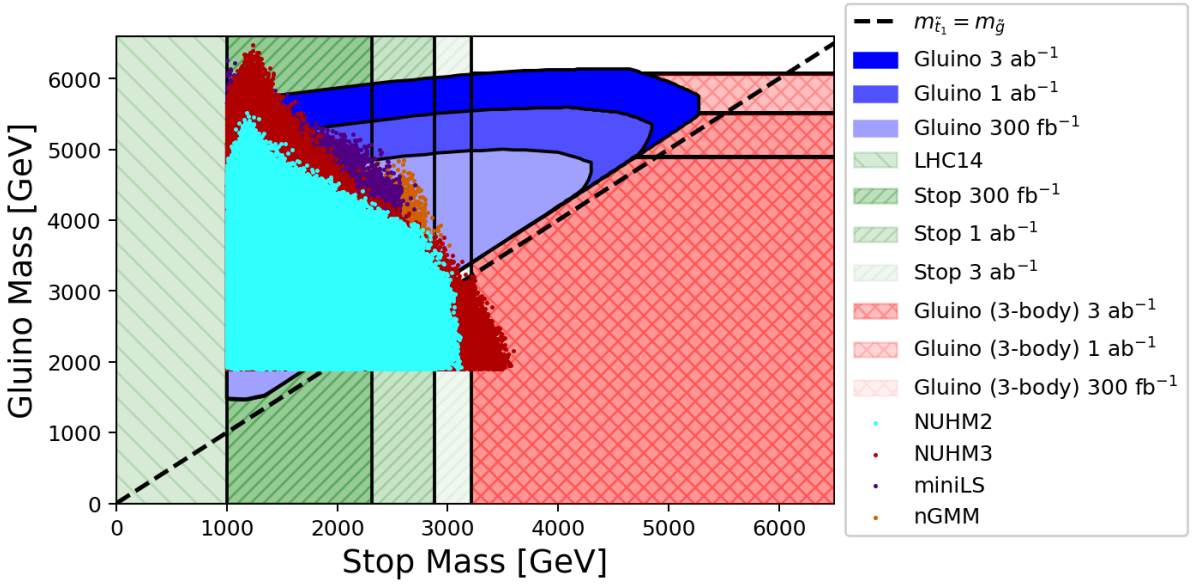

Figure 18: Points with $\Delta_{\rm EW} < 30$ in the stop-gluino mass plane from dedicated scans of the NUHM2, NUHM3, nGMM and mini-landscape models described in Sec. 5. These are plotted along with (i) the projected 5σ stop reach of LHC33 from Fig. 9, (ii) the projected 5σ gluino reach of LHC33 from Fig. 10 obtained assuming that the gluino decays via $\tilde{g} \to \tilde{t}_1\bar{t}, \tilde{t}_1^* t$, and (iii) the projected 5σ LHC33 reach for gluino pairs from Fig. 11 obtained assuming that the gluino decays via off-shell stops and sbottoms. The 95% CL exclusion lines are typically $400 - 500$ GeV higher.

5.2 The Reach of LHC33 for Natural SUSY Models

We have already mentioned that in the natural NUHM2 model, the SSdB signal from wino pair production, together with the monojet plus soft dilepton signal, are sufficient to probe essentially the entire $\Delta_{\rm EW} < 30$ region of the phenomenologically viable parameter space of the model at the HL-LHC. As already stressed, the model characteristics crucial for arriving at this conclusion are 1) gaugino mass unification and 2) the naturalness upper limit $m_{\tilde{g}} \lesssim 5$ TeV on the gluino mass, which implies a corresponding limit on the wino mass. The existence of well-motivated natural SUSY models where one of these conditions is not satisfied was one of our main motivations for studying the gluino and top squark reach at LHC33.

With this in mind, we begin by showing a scatter plot of the stop versus gluino mass in Fig. 18 for the four models discussed in Sec. 5.1: natural NUHM2 (cyan/ lightest), natural NUHM3 (dark red/ second darkest), natural mini-landscape (purple/ darkest) and nGMM (orange/ second lightest). For each model, we have scanned the parameter space consistent with the Higgs mass as well as LHC sparticle mass constraints ($m_{\tilde{g}} > 1.9$ TeV) and placed a symbol in the figure if we find a solution compatible with $\Delta_{\rm EW} < 30$. For the sake of brevity, we will not describe the details of the scans here, but refer the reader to our earlier studies of the NUHM model [15], the nGMM model [55], and the natural mini-landscape picture [60],

where the parameter space of each model is also detailed.[15] Also shown are the regions of the stop-gluino mass plane accessible via searches for stop or gluino pair production at LHC33 using the strategies described in Sec. 4.[16]

Since both gluinos and stops decay essentially with the branching fractions assumed in our simplified model analyses of Sec. 4, the reach results that we obtained there should be directly applicable. In particular, LHC33 experiments should be able to discover stops with a $\geq 5\sigma$ significance for $m_{\tilde{t}_1} < 2.3$ (2.8) [3.2] TeV, assuming an integrated luminosity of 0.3 (1.0) [3.0] ab^{-1}: *i.e.*, to the left of the correspondingly labelled lines in the figure. Also shown are the corresponding discovery contours for the gluino. For heavy stops, these extend to 5.5 TeV for an integrated luminosity of 1 ab^{-1} and beyond 5 TeV if the stop is just 1 TeV (in which case it would be easily discovered at the 14 TeV LHC). We have not shown the 95% CL contours here, but these exclusion limits typically extend $400 - 500$ GeV beyond the discovery reaches shown in the figure.

The following features of Fig. 18 are particularly worth noting:

1. We see that at least one of the gluino or the stop should be discoverable at LHC33 even with an integrated luminosity of 300 fb^{-1} for all viable models with $\Delta_{\rm EW} < 30$.

2. For the anticipated LHC33 integrated luminosity of 1 ab^{-1}, there should be a signal in *both* gluino as well as stop pair production channels for most of the parameter space with $\Delta_{\rm EW} < 30$.

3. If an integrated luminosity of 3 ab^{-1} (the integrated luminosity expected at the HL-LHC) is accumulated at LHC33, both gluino and stop signals should be observable for essentially all natural SUSY models, the exceptions being the regions with either $m_{\tilde{t}_1} < 1.3$ TeV (in which case the stop should have been already discovered at the HL-LHC), or the region with $m_{\tilde{g}} < 3.2$ TeV, much of which would be probed at the HL-LHC where the 5σ reach extends to 2.8 TeV.

4. As mentioned above, $m_{\tilde{g}}$ is bounded above for all models. This bound is roughly model-independent for values of $m_{\tilde{t}_1} \gtrsim 2$ TeV, but for lighter stops, $m_{\tilde{g}}$ can be significantly larger, extending to as high as 6 TeV especially in the NUHM3 and the mini-landscape models where the first and second generation sfermions are much heavier than the third generation sfermions. For these models, the increase in stop masses from heavy gluino loops (which results in too large of a $\Delta_{\rm EW}$) is compensated by negative two loop contributions due to heavy first/generation. This effect is clearly smaller in models where the high scale third generation mass is not independent of other scalar masses, resulting in a tighter naturalness bound on $m_{\tilde{g}}$.

The take-away message from this figure is that over the entire range of natural SUSY models with $\Delta_{\rm EW} < 30$, experiments at LHC33, with an integrated luminosity of 1 ab^{-1}, will have the

[15] Aside from the broad scans that yield a wide range of $\Delta_{\rm EW}$ in these papers, we have also carried out focussed scans targetting the low $\Delta_{\rm EW}$ region to obtain accurate naturalness bounds on stop and gluino masses.

[16] For the case $m_{\tilde{t}_1} + m_t > m_{\tilde{g}}$, we assume that the reach is essentially independent of $m_{\tilde{t}_1}$. We expect this to be the case except, perhaps, very close to the kinematic boundary for gluino two-body decays.

sensitivity to discover at least one of the stop or the gluino – and over much of the parameter space, both. In models with gaugino mass unification, there will likely be observable signatures in the SSdB channel[17] and perhaps also in other channels because the $\widetilde{Z}_2$ decays will lead to an excess of soft dilepton pairs with $m_{\ell\ell} < m_{\widetilde{Z}_2} - m_{\widetilde{Z}_1}$ in events triggered by hard jets or large $E_T^{\rm miss}$.

The reader may be concerned that the analysis that we have presented is specific to the models examined in the study. We should mention that these models encompass a wide range of models with the superpartner content of the MSSM. Our results for the reach for gluinos and stops are unlikely to be significantly altered in natural SUSY models from our projections, since these projections depend essentially on the production cross sections and on the decay patterns. The latter depend on the existence of light higgsinos and on the fact that third generation squarks are significantly lighter than other squarks.[18] It is also difficult to envision how the upper limits on gluino and stop masses obtained from $\Delta_{\rm EW} < 30$ could be significantly altered from those in the NUHM3 RNS model, where the high scale third generation squark and gluino masses can be chosen independently. The NUHM3 bound on $m_{\tilde{g}}$ is unlikely to be very sensitive to the gaugino mass unification assumption. This is confirmed by the fact that the distributions of points for the NUHM3 model and for the mini-landscape model are qualitatively similar. We therefore conclude that LHC33 experiments should be able to discover natural SUSY (as we have defined it) in all models with a minimal superpartner spectrum. The absence of any signal[19] will mean that even though weak scale SUSY may resolve the big hierarchy problem, a little hierarchy would remain (*i.e.* SUSY would contain significant electroweak fine-tuning).

6 Summary and Concluding Remarks

We have examined the proposed LHC33 reach for SUSY via stop and gluino pair production signals (assuming that higgsinos are the lightest SUSY particles with masses not much larger than m_Z) assuming an integrated luminosity of $\sim 0.3 - 3$ ab^{-1}. For our analyses, we assume that the stop decays to higgsino-like charginos and neutralinos via $\tilde{t}_1 \to t\widetilde{Z}_{1,2}$ and $\tilde{t}_1 \to b\widetilde{W}_1$, and that the gluino decays via $\tilde{g} \to t\tilde{t}_1$ or via the three-body decays $\tilde{g} \to t\bar{t}\widetilde{Z}_{1,2}, tb\widetilde{W}_1$. In this study, we conservatively assume that the decay products of the higgsino-like $\widetilde{W}_1$ and $\widetilde{Z}_2$ are too soft to be detected.

We believe that our analysis with the assumed stop and gluino decay patterns is strongly motivated by rather conservative naturalness arguments that imply spectra with gluinos may be as heavy as 6 TeV and light stops as heavy as 3 TeV can be natural as long as higgsinos are lighter than ~ 350 GeV. Gluino and stops may then be well beyond the discovery reach of even the HL-LHC which extends to $m_{\tilde{g}} \lesssim 2.8$ TeV and $m_{\tilde{t}_1} < 1.2$ TeV, while signals from electroweak

[17] In Ref. [15] we had projected that the HL-LHC would probe the entire natural parameter space via the SSdB signature. Since then, we have discovered small additional backgrounds and also (via more dedicated scans) found that the gluino mass bound extends somewhat beyond 4.5 TeV (see Fig. 18) that we projected in our earlier study. HL-LHC experiments should nonetheless be able to discover SUSY over much of the parameter space of this model.

[18] If first/second generation squarks are also light, their production would enhance the SUSY signal and likely offer additional channels to search for SUSY.

[19] Recall that the 95% CL exclusion contours are typically 0.5 TeV beyond the 5σ discovery contours in Fig. 18.

production of higgsinos may be buried below SM backgrounds if these are essentially degenerate. Indeed, there are theoretically well-motivated natural SUSY models with compressed gaugino spectra (see Sec. 5.1) where SUSY may completely elude detection at the HL-LHC. Readers who do not subscribe to these naturalness arguments should view our study as an analysis of the SUSY reach of the proposed energy upgrade of the LHC for models with light higgsinos.

Our optimized cuts to extract the stop production signal at LHC33 are listed in (6) while the corresponding cuts for the gluino production signal are shown in (11). From our results for the stop cross section after cuts shown in Fig. 9, we project that LHC33 experiments should be able to discover stops at 5σ level with a mass values up to 2.3 (2.8) [3.2] TeV, assuming an integrated luminosity of 0.3 (1) [3] ab^{-1}. If no signal is seen, the 95% CL exclusion limits extend about 600 GeV further. The gluino reach of LHC33 is illustrated in Fig. 10 assuming that gluinos decay via $\tilde{g} \to t\tilde{t}_1$ and in Fig. 11 for the case that gluinos decay to third generation quarks plus higgsinos. In both cases we find that LHC33 experiments should be able to discover a gluino at 5σ level for $m_{\tilde{g}}$ as heavy as 5 (5.5) [6] TeV assuming an integrated luminosity of 0.3 (1) [3] ab^{-1}. The 95% CL exclusion reach values are typically 400-500 GeV higher than the 5σ values.

In Sec. 5, we have examined the implications of our gluino and stop reach results for natural SUSY models, defined to have no worse than 3% electroweak fine-tuning. We have stressed that electroweak naturalness is a very conservative approach to fine-tuning in that it allows for the possibility that underlying model parameters (usually taken to be independent) might be correlated in the underlying theory. Disregarding this may prematurely cause us to discard perfectly viable models because they appear to be unnatural in an effective theory. Even with this conservative approach, we find that experiments at LHC33 will be able to discover either the stop or the gluino even with an integrated luminosity of 300 fb^{-1} in *all natural SUSY models* where the low energy theory is the MSSM. With an integrated luminosity of 1-3 ab^{-1}, for the bulk of the models, both gluino and stop signals should be observable, together perhaps with some additional signals for specific scenarios: see Fig. 18. This is in sharp contrast to the HL-LHC, where signals from natural SUSY models with compressed gaugino masses may well remain undiscovered because gluinos, stops, and winos are too heavy and higgsino signals are buried under SM backgrounds. LHC33 will, therefore, allow an unambiguous test of natural SUSY models, conservatively defined by spectra with no worse than 3% electroweak fine-tuning.

Acknowledgments

We acknowledge useful communications with T. Cohen. This work was supported in part by the US Department of Energy, Office of High Energy Physics; was aided by the use of SLAC Computing Resources; and was performed in part at the Aspen Center for Physics, which is supported by National Science Foundation grant PHY-1607611.

References

[1] E. Witten, Nucl. Phys. B **188**, 513 (1981); R. K. Kaul, Phys. Lett. B **109**, 19 (1982).

[2] S. Dimopoulos, S. Raby and F. Wilczek, Phys. Rev. D **24** (1981) 1681; U. Amaldi, W. de Boer and H. Furstenau, Phys. Lett. B **260**, 447 (1991); J. R. Ellis, S. Kelley and D. V. Nanopoulos, Phys. Lett. B **260** (1991) 131; P. Langacker and M. X. Luo, Phys. Rev. D **44** (1991) 817.

[3] L. E. Ibañez and G. G. Ross, Phys. Lett. **B110**, 215 (1982); K. Inoue *et al.* Prog. Theor. Phys. **68**, 927 (1982) and **71**, 413 (1984); L. Ibañez, Phys. Lett. **B118**, 73 (1982); H. P. Nilles, M. Srednicki and D. Wyler, Phys. Lett. B **120** (1983) 346; J. Ellis, J. Hagelin, D. Nanopoulos and M. Tamvakis, Phys. Lett. **B125**, 275 (1983); L. Alvarez-Gaumé. J. Polchinski and M. Wise, Nucl. Phys. **B221**, 495 (1983); B. A. Ovrut and S. Raby, Phys. Lett. B **130** (1983) 277; for a review, see L. E. Ibanez and G. G. Ross, Comptes Rendus Physique **8** (2007) 1013.

[4] G. Aad *et al.* [ATLAS Collaboration], Phys. Lett. B **716** (2012) 1; S. Chatrchyan *et al.* [CMS Collaboration], Phys. Lett. B **716** (2012) 30.

[5] H. E. Haber and R. Hempfling, Phys. Rev. Lett. **66** (1991) 1815; J. R. Ellis, G. Ridolfi and F. Zwirner, Phys. Lett. B **257** (1991) 83; Y. Okada, M. Yamaguchi and T. Yanagida, Prog. Theor. Phys. **85** (1991) 1; For a review, see *e.g.* M. S. Carena and H. E. Haber, Prog. Part. Nucl. Phys. **50** (2003) 63 [hep-ph/0208209].

[6] ATLAS collaboration, ATLAS-CONF-2017-022; CMS Collaboration, CMS-SUS-16-036.

[7] ATLAS Collaboration, ATLAS-CONF-2017-039; CMS Collaboration, CMS-16-034.

[8] ATLAS Collboration, ATLAS-CONF-2017-020; CMS Collboration, CMS-SUS-16-051 and CMS-SUS-16-049.

[9] ATLAS Collboration, ATLAS-CONF-2017-021; CMS Collboration, CMS-SUS-16-051.

[10] See, *e.g.* ATLAS Phys. PUB 2013-011; CMS Note-13-002.

[11] Y. Gershtein *et al.*, arXiv:1311.0299 [hep-ex].

[12] `https://twiki/cern.ch/bin/view/AtlasPublic/UpgradePhysicsStudies`

[13] H. Baer, V. Barger, J. S. Gainer, P. Huang, M. Savoy, D. Sengupta and X. Tata, Eur. Phys. J. C **77** (2017) 499, arXiv:1612.00795 [hep-ph].

[14] H. Baer, V. Barger, P. Huang, D. Mickelson, A. Mustafayev, W. Sreethawong and X. Tata, Phys. Rev. Lett. **110** (2013) no.15, 151801.

[15] H. Baer, V. Barger, P. Huang, D. Mickelson, A. Mustafayev, W. Sreethawong and X. Tata, JHEP **1312** (2013) 013.

[16] H. Baer, V. Barger, D. Mickelson, A. Mustafayev and X. Tata, JHEP **1406** (2014) 172.

[17] H. Baer, V. Barger, P. Huang and X. Tata, JHEP **1205** (2012) 109.

[18] H. Baer, V. Barger, P. Huang, A. Mustafayev and X. Tata, Phys. Rev. Lett. **109** (2012) 161802.

[19] H. Baer, V. Barger, P. Huang, D. Mickelson, A. Mustafayev and X. Tata, Phys. Rev. D **87** (2013) 11, 115028.

[20] O. Bruenning, O. Dominguez, S. Myers, L. Rossi, E. Todesco and F. Zimmerman, arXiv:1108.1617 [phys.acc-ph].

[21] H. Baer *et al.* arXiv:1702.06588 [hep-ph].

[22] T. Cohen, T. Golling, M. Hance, A. Henrichs, K. Howe, J. Loyal, S. Padhi and J. G. Wacker, arXiv:1310.0077 [hep-ph]; T. Cohen, T. Golling, M. Hance, A. Henrichs, K. Howe, J. Loyal, S. Padhi and J. G. Wacker, JHEP **1404** (2014) 117.

[23] J. Alwall, M. Herquet, F. Maltoni, O. Mattelaer and T. Stelzer, JHEP **1106** (2011) 128; J. Alwall, R. Frederix, S. Frixone, V Herschi, F. Maltoni, O. Mattelaer, H.-S. Shao, T. Stelzer, P. Torrielli and M. Zaro, JHEP **1407** (2014) 079.

[24] T. Sjostrand, S. Mrenna and P. Z. Skands, Comput. Phys. Commun. **178** (2008) 852.

[25] J. de Favereau *et al.* [DELPHES 3 Collaboration], JHEP **1402** (2014) 057.

[26] M. Cacciari, G. P. Salam and G. Soyez, JHEP **0804**, 063 (2008) [arXiv:0802.1189 [hep-ph]].

[27] M. Cacciari, G. P. Salam and G. Soyez, Eur. Phys. J. C **72**, 1896 (2012) [arXiv:1111.6097 [hep-ph]].

[28] CMS Collaboration [CMS Collaboration], CMS-PAS-BTV-15-001.

[29] M. Cacciari and G. P. Salam, Phys. Lett. B **659**, 119 (2008) [arXiv:0707.1378 [hep-ph]].

[30] S. Corréad, V. Kostioukine, J. Levêque, A. Rozanov, J. B. de Vivie, ATLAS Note, ATLAS-PHYS-2004-006, and V. Kostioukine, ATLAS Note, ATLAS-PHYS-2003-033.

[31] `https://twiki.cern.ch/twiki/bin/view/LHCPhysics/SUSYCrossSections`; C. Borschensky, M. Krmer, A. Kulesza, M. Mangano, S. Padhi, T. Plehn and X. Portell, Eur. Phys. J. C **74**, no. 12, 3174 (2014) doi:10.1140/epjc/s10052-014-3174-y [arXiv:1407.5066 [hep-ph]].

[32] `https://twiki.cern.ch/twiki/bin/view/LHCPhysics/HiggsEuropeanStrategy` (Accessed August 18, 2017.)

[33] M. Aliev, H. Lacker, U. Langenfeld, S. Moch, P. Uwer and M. Wiedermann, "HATHOR: HAdronic Top and Heavy quarks cross section calculatoR," Comput. Phys. Commun. **182**, 1034 (2011) doi:10.1016/j.cpc.2010.12.040 [arXiv:1007.1327 [hep-ph]]; P. Kant, O. M. Kind, T. Kintscher, T. Lohse, T. Martini, S. Mölbitz, P. Rieck and P. Uwer, "HatHor for single top-quark production: Updated predictions and uncertainty estimates for single top-quark production in hadronic collisions," Comput. Phys. Commun. **191**, 74 (2015) doi:10.1016/j.cpc.2015.02.001 [arXiv:1406.4403 [hep-ph]].

[34] A. Bredenstein, A. Denner, S. Dittmaier and S. Pozzorini, JHEP **1003**, 021 (2010) [arXiv:1001.4006 [hep-ph]].

[35] A. Bredenstein, A. Denner, S. Dittmaier and S. Pozzorini, Phys. Rev. Lett. **103** (2009) 012002.

[36] F. Febres Cordero, L. Reina and D. Wackeroth, Phys. Rev. D **80** (2009) 034015 [arXiv:0906.1923 [hep-ph]].

[37] G. Bevilacqua and M. Worek, JHEP **1207**, 111 (2012) doi:10.1007/JHEP07(2012)111 [arXiv:1206.3064 [hep-ph]].

[38] `https://twiki.cern.ch/twiki/bin/view/LHCPhysics/SingleTopRefXsec` (Accessed August 18, 2017.)

[39] ATLAS Collaboration, ATLAS-CONF-2016-052.

[40] For a discussion of gluino production as a contaminator of the stop signal, see R. Kadala, P. Mercadante, J. Mizukoshi and X. Tata, Eur. Phys. J. C **56** (2008) 511.

[41] R. Barbieri and G. F. Giudice, Supersymmetric Particle Masses," Nucl. Phys. B **306**, 63 (1988); this measure was first introduced in J. R. Ellis, K. Enqvist, D. V. Nanopoulos and F. Zwirner, Superstring Models," Mod. Phys. Lett. A **1**, 57 (1986).

[42] H. Baer, V. Barger and D. Mickelson, Phys. Rev. D **88**, (2013) 095013; A. Mustafayev and X. Tata, Indian J. Phys. **88** (2014) 991.

[43] H. Baer, V. Barger and M. Savoy, Phys. Rev. D **93** (2016) 3, 035016.

[44] H. Baer, V. Barger, J. S. Gainer, P. Huang, M. Savoy, H. Serce and X. Tata, arXiv:1702.06588 [hep-ph].

[45] D. Matalliotakis and H. P. Nilles, Nucl. Phys. B **435** (1995) 115; M. Olechowski and S. Pokorski, Phys. Lett. B **344** (1995) 201; P. Nath and R. L. Arnowitt, Phys. Rev. D **56** (1997) 2820; J. Ellis, K. Olive and Y. Santoso, Phys. Lett. **B539** (2002) 107; J. Ellis, T. Falk, K. Olive and Y. Santoso, Nucl. Phys. **B652** (2003) 259; H. Baer, A. Mustafayev, S. Profumo, A. Belyaev and X. Tata, JHEP**0507** (2005) 065.

[46] H. Baer, V. Barger and M. Savoy, Phys. Rev. D **93** (2016) no.7, 075001.

[47] L. Girardello and M. T. Grisaru, Nucl. Phys. B **194** (1982) 75, and recently re-emphhasized by G. G. Ross, K. Schmidt-Hoberg and F. Staub, Phys. Lett. B **759** (2016) 110.

[48] T. Cohen, J. Kearney and M. Luty, Phys. Rev. D **91** (2014) 075004; A. Nelson and T. Roy, Phys. Rev. Lett. **114** (2015) 201802; S. P. Martin, Phys. Rev. D **92** (2015) 035004.

[49] C. Brust, A. Katz, S. Lawrence and R. Sundrum, JHEP **1203** (2012) 103.

[50] P. Schwaller and J. Zurita, JHEP **1403**, 060 (2014); Z. Han, G. D. Kribs, A. Martin and A. Menon, Phys. Rev. D **89** (2014) no.7, 075007; H. Baer, A. Mustafayev and X. Tata, Phys. Rev. D **90** (2014) no.11, 115007; C. Han, D. Kim, S. Munir and M. Park, JHEP **1504** (2015) 132.

[51] K. Choi, A. Falkowski, H. P. Nilles, M. Olechowski and S. Pokorski, J. High Energy Phy**0411**, 076 (2004); K. Choi, A. Falkowski, H. P. Nilles and M. Olechowski, Nucl. Phys. **B718**, 113 (2005). J. P. Conlon, F. Quevedo and K. Suruliz, JHEP **0508**, 007 (2005) [arXiv:hep-th/0505076].

[52] S. Kachru, R. Kallosh, A. Linde and S. P. Trivedi, Phys. Rev. **D68**, 046005 (2003).

[53] K. Choi and H. P. Nilles, JHEP **0704**, (2007) 006 stress the robustness of the gaugino mass relation in MM models. See also, O. Lebedev, V. Löwen, Y. Mambrini, H. P. Nilles ad M. Ratz, JHEP **0702** (2007) 063; E. Dudas, C. Papineau and S. Pokorski, JHEP **0702** (2007) 028, and H. Abe, T. Higaki and Y. Omura, Phys. Rev. D **75** (2007) 025019.

[54] H. Baer, V. Barger, D. Mickelson and M. Padeffke-Kirkland, Phys. Rev. D **89**, 115019 (2014).

[55] H. Baer, V. Barger, H. Serce and X. Tata, Phys. Rev. D **94** (2016) 115017.

[56] ISAJET 7.85, by H. Baer, F. Paige, S. Protopopescu and X. Tata, hep-ph/0312045; Isasugra, by H. Baer, C. H. Chen, R. B. Munroe, F. E. Paige and X. Tata, Phys. Rev. D **51** (1995) 1046.

[57] H. P. Nilles and P. K. S. Vaudrevange, Adv. Ser. Direct. High Energy Phys. **22** (2015) 49.

[58] H. P. Nilles, Adv. High Energy Phys. **2015** (2015) 412487.

[59] S. Krippendorf, H. P. Nilles, M. Ratz and M. W. Winkler, Phys. Lett. B **712** (2012) 87 [arXiv:1201.4857 [hep-ph]]; M. Badziak, S. Krippendorf, H. P. Nilles and M. W. Winkler, J. High Energy Phys. **1303** 094 (2013).

[60] H. Baer, V. Barger, M. Savoy, H. Serce and X. Tata, JHEP **1706** (2017) 101.